Journal of Molecular Structure 1276 (2023) 134769

Contents lists available at ScienceDirect

Journal of Molecular Structure

journal homepage: www.elsevier.com/locate/molstr

Electrochemical and *in-situ* spectroelectrochemical properties of novel (5-(tert-butyl)-2-((3,4-dicyanophenoxy)methyl)phenyl)methanolate substituted mononuclear metal phthalocyanines

Safinaz Şahin, Özgün Akdağ, Efe Baturhan Orman, Zafer Odabaş*, Ali Rıza Özkaya

Department of Chemistry, Marmara University, Göztepe, Istanbul 34722, Turkey

ARTICLE INFO

Article history:
Received 2 September 2022
Revised 16 November 2022
Accepted 7 December 2022
Available online 11 December 2022

Keywords:
Ball-type phthalocyanine precursors
Synthesis
Cyclic voltammetry
In situ electrocolorimetry
In situ spectroelectrochemistry

ABSTRACT

This work involves the synthesis and characterization of metallic (Co, Fe, Mn, Ni, Zn) ball-type phthalocyanine precursors by using novel 4,4′-(((4-(tert-butyl)-1,2-phenylene)bis-(methylene))bis(oxy)) diphthalonitrile starting compound. The classical oxo-bridge in phthalocyanines was altered with the -OCH_2- bridge first time for these ball-type phthalocyanine precursors, and the effects of this change on the chemical, physical and spectral features of phthalocyanine complexes were investigated, in the study. The redox properties of phthalocyanines were researched by electrochemical and *in situ* spectroelectrochemical measurements on a Pt working electrode in non-aqueous medium. The color changes involved in the redox processes were observed via *in situ* electrocolorimetric techniques. Electrochemical and UV–Vis spectral measurements exhibited that the compounds had reversible and serial one-electron reduction and oxidation processes. Furthermore, they also had nitrile reduction processes because of opened nitrile groups located at peripheral tails of the phthalocyanine complexes. The plentiful redox conducts of the complexes such as Pc ring based and/or central redox active metal-based reduction and oxidation reactions at low potentials showed that these complexes can be used as functional materials. Because of the apparent spectral and net color changes, the complexes are suitable for utilization in electrochromic devices. Moreover, their rich redox features are a sign of their high electrocatalytic activity for oxygen reduction.

1. Introduction

Metallo and metal-free phthalocyanine (Pc) complexes are biaromatic heterocyclic macromolecules that have attracted great interest in recent years. Due to their aromaticity originating from the conjugated 18-π electron systems in the inner ring, they are extremely stable physically, chemically, and spectrally, and thus have a wide variety of electronic, electrical, electrochemical, and optical properties [1]. Pc complexes are very valuable chemicals due to their unique properties mentioned above and are involved in many applications such as dyes [2], conductive materials [3], solar cell systems, optical/electronic/optoelectronic materials [4–6], sensors [7], photodynamic therapy (PDT) agent [8], electrocatalyst [9], electrochromic devices [10], photovoltaic devices [11] and electrochemical energy conversion and storage systems (cell/battery systems) [12] in various technological fields. Pc variants with different features can be designed efficiently by adjusting synthetic procedures, by changing the type/number/linkage bridge of substituents in peripheral and non-peripheral positions of their outer rings (aromatic phenyl rings), or by using metals with different coordination numbers in the center. Thus, since newly synthesized metal Pc complexes have become more attractive in technological applications, investigations on these compounds have been continuing effectively for about 115 years [13]. As an alternative starting material to the phthalonitrile, Pc researchers started to use diphthalonitrile compounds for the first time in the early 2000s, for classical Pc synthesis. The expectation was the formation of a classical mononuclear Pc from two molecules of this new starting compound. However, contrary to expectations, the reaction resulted not only with this predicted product, but also with the other two different types of phthalocyanine compounds from four molecules of diphthalonitrile, in some cases the formation of a mononuclear Pc with eight nitrile end groups [14–16] and sometimes a dinuclear Pc involving two mononuclear Pc units connected to each other by four organic bridges [17,18], depending on the nature of the starting material and reaction conditions. The mononuclear Pc including eight nitrile groups has brought great innovation to Pc research in two different ways. Firstly, the CN

* Coresponding author.
E-mail address: zodabas@marmara.edu.tr (Z. Odabaş).

https://doi.org/10.1016/j.molstruc.2022.134769
0022-2860/

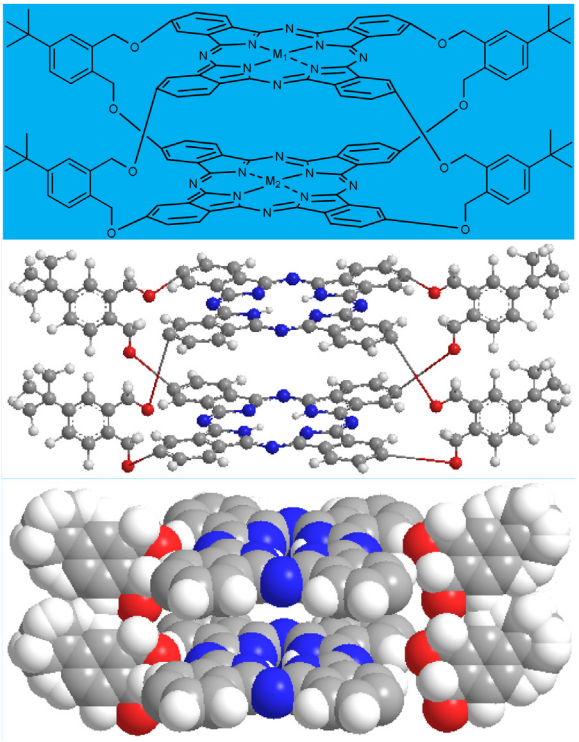

Scheme 1. The molecular shapes and 3D structures of the ball type Pc complexes.

Mononuclear Pc Complexes	Redox Processes	Process
CoPc (in DMSO)	$Co(II)Pc(-2)/[Co(III)Pc(-2)]^{+}$	O1
	$Co(II)Pc(-2)/[Co(I)Pc(-2)]^{-}$	R1
	$[Co(I)Pc(-2)]^{-}/[Co(I)Pc(-3)]^{2-}$	R2
ZnPc (in DMSO)	$Zn(II)Pc(-2)/[Zn(II)Pc(-1)]^{+}$	O1
	$Zn(II)Pc(-2)/[Zn(II)Pc(-3)]^{-}$	R1
	$[Zn(II)Pc(-3)]^{-}/[Zn(II)Pc(-4)]^{2-}$	R2
	$[Zn(II)Pc(-4)]^{2-}/[Zn(II)Pc(-5)]^{3-}$	R3
Dinuclear Ball-type Pc Complexes	**Redox Processes**	**Process**
Co_2Pc_2 (in DMSO)	$[Co(II)Pc(-2)]_2/[Co(II)Pc(-2).Co(II)Pc(-1)]^{+}$	O1
	$[Co(II)Pc(-2)]_2/[Co(II)Pc(-2)]Co(I)Pc(-2)]^{-}$	R1
	$[Co(II)Pc(-2)]Co(I)Pc(-2)]^{-}/[Co(I)Pc(-2)]_2^{2-}$	R2
	$[Co(I)Pc(-2)]_2^{2-}/[Co(I)Pc(-2).Co(I)Pc(-3)]_2^{3-}$	R3
	$[Co(I)Pc(-2).Co(I)Pc(-3)]_2^{3-}/[Co(I)Pc(-3)]_2^{4-}$	R4
Zn_2Pc_2 (in DMSO)	$[Zn(II)Pc(-2)]_2/[Zn(II)Pc(-1)]_2^{2+}$	O1
	$[Zn(II)Pc(-2)]_2/[Zn(II)Pc(-3)]_2^{2-}$	R1
	$[Zn(II)Pc(-3)]_2/[Zn(II)Pc(-4)]_2^{4-}$	R2
	$[Zn(II)Pc(-4)]_2/[Zn(II)Pc(-5)]_2^{6-}$	R3
	$[Zn(II)Pc(-5)]_2/[Zn(II)Pc(-6)]_2^{8-}$	R4

Scheme 2. The representative redox processes of mononuclear and dinuclear ball-type Pc complexes.

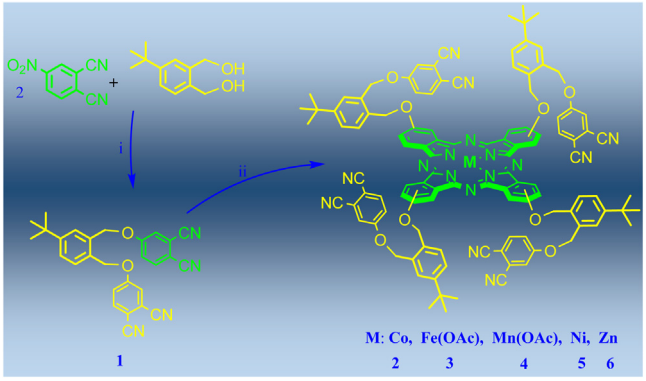

Scheme 3. Synthesis of phthalonitrile compound (1) and MPcs (2–6), Reagents and conditions: (i) N_2, K_2CO_3, dry DMF, 55 °C, 24 h. (ii) N_2, $Co(OAc)_2.4H_2O$, $Fe(OAc)_2$, $Mn(OAc)_2.4H_2O$, $NiCl_2$ and $Zn(OAc)_2.4H_2O$, DMF, DBU, at reflux temp., 12 h.

groups in this compound are redox-active and reduced themselves. In addition, nitrile groups are very strongly electron withdrawing and thus, Pc compound involving these groups at the end are easily reduced with respect to many other Pc compounds.

On the other hand, if desired, the mononuclear ball-type Pc precursor with the eight nitrile groups can be used to obtain homo or hetero dinuclear ball-type phthalocyanines (Pcs) (Scheme 1) when suitable reaction conditions are provided. Therefore, it can be used as a high-tech material with very different features from classical Pcs [17–22].

It can be inferred from the previous studies that the mononuclear Pcs and the dinuclear ball-type Pcs have different redox behaviors. As shown in Scheme 1, there are two identical Pc rings in the ball-type molecular structure. Because of the presence of two identical Pc rings in one M_2Pc_2 unit, ball-type phthalocyanines have richer redox features than mononuclear Pcs. Scheme 2 shows and compares the redox behaviors of mononuclear and dinuclear ball-type Pc complexes. If we consider the first reduction process, this process may split into two processes or involve the reduction of two Pc rings at the same potential without splitting [23–25].

In this study, the ball-type metallo (Co, Fe, Mn, Ni, Zn) Pc precursors have been synthesized using 4,4′-(((4-(tert-butyl)−1,2-phenylene)bis(methylene))bis(oxy))diphthalonitrile as the starting compound (Scheme 3). Since the Pcs are peripherally tetrasubstituted derivatives, each Pcs (2–6) contained a mixture of four positional isomers, which would have the following symmetry groups: D2h, C4h, C2v, and Cs [26]. Thus, the image in Scheme 3 suggests that the terminal oxygen reacts to the joint to the lateral aromatic ring of the Pcs, however, the representation shows there is a bond between this oxygen atom and the ring but does not clarify the position. Additionally, the -OCH_2- the bridge was used instead of the oxo bridge which was used in traditional Pcs for the first time in ball-type Pc precursor compounds, and the effects of this change on the chemical, physical and spectral properties of Pc complexes were investigated.

MN_4 macrocyclic compounds have electroactive multiple reversible redox processes and may behave as electron transfer intermediaries [27]. Pcs have rich redox behaviors such as; reversible redox processes, multi-electron transfer, and redox peaks at low potentials. These features are desired properties for electrochromic applications. Moreover, the increased redox richness of the complexes directly affects the spectral changes caused by the redox reactions [28]. There is a near and heavy relation between the molecular structure and the rich redox features of a phthalocyanine compound. Redox properties of Pcs determine the applicability in the electrochemical technological areas [29]. Modifications of Pcs with functional groups expand the redox richness and flexibility in different electrochemical applications [30]. Many alternatives for the Pc compounds can be designed by using various central metals and substituents (peripheral, nonperipheral, axial, tetra, or octa substitution), to enrich the redox properties [31]. To use Pcs complexes efficiently, characteristic redox features of novel Pc compounds that include redox active and inactive metal (M) centers, should be investigated accurately. When similarities in the general redox behaviors of MPc compounds are examined, it is clearly understood that the behaviors of both redox inactive and redox active metal-centered complexes are quite similar to each other. For the inactive metal-centered Pc com-

plexes, all oxidation and reduction redox processes happen on the Pc ring. However, redox active metal-centered compounds display both metal-centered and ring-centered electron deliver mechanisms because redox active metals have various half-filled and/or empty d orbitals in the HOMO-LUMO gap. Complexes with such a rich and low potential redox conduct generally have the potential to own higher electrocatalytic activity, and elucidation of electrochemical redox attitudes of them is of great importance in this respect [32,33].

This research focuses on the effects of metal centers on the redox properties of novel phthalocyanine complexes. It is different from the early studies because it aimed to systematically compare the redox properties of Pcs that had redox active and inactive metal centers, and CN groups end of the tail of molecular structure. Metal centers, substitution positions, and substituted groups directly affect the redox properties. So as to make a good comparison of the effects of metal centers on the redox properties; redox active metals (iron, cobalt, manganese) and redox inactive metals (nickel and zinc) were chosen in this work. To exactly describe the characteristic redox properties of Pcs, electrochemical, *in situ* electrocolorimetric, and *in situ* spectroelectrochemical techniques were also used.

The major aim of this research is to discover the role of the metal-centered on the Pc ring in redox processes by establishing particular relations between electrochemical and spectroelectrochemical results. In the light of this approach, electrochemical redox attitudes of novel Pc complexes (CoPc (2), Fe(OAc)Pc (3), Mn(OAc)Pc (4), NiPc (5), and ZnPc (6) were examined by using square wave voltammetry (SWV), cyclic voltammetry (CV), and controlled potential coulometry (CPC) techniques.

2. Experimental

In this study, 4,4′-(((4-(tert-butyl)−1,2-phenylene)bis(methylene))bis(oxy))diphthalonitrile (1) have been synthesized nucleophilic aromatic substitution reaction of sodium (4-(tert-butyl)−1,2-phenylene)dimethanolate and 4-nitrophthalonitrile, and novel metallophthalocyanine compounds (CoPc (2), Fe(OAc)Pc (3), Mn(OAc)Pc (4), NiPc (5), and ZnPc (6)) have been achieved by using the starting compound (Scheme 3). The used materials, equipment, and Matrix-Assisted Laser Desorption/Ionization (MALDI) sample preparation are given as supplementary information section.

2.1. Synthesis of sodium (4-(tert-butyl)−1,2-phenylene)dimethanolate [34]

2.32 g (61 mmol) $LiAlH_4$ was mixed with 40 mL diethylether and then 1.08 g (5 mmol) 5–*tert*-butylphthalic anhydride was dissolved in 40 mL diethyl ether. The prepared second solution was adjoined to the first solution dropwise. Then, after the reaction concoction was stirred at room conditions for 10–15 min, the reaction was terminated as it was understood from the thin layer chromatography (TLC) of the reaction mixture that the starting materials were consumed. After the solids in the reaction mixture are filtered off and 390 mg (10 mmol) of $NaNH_2$ were adjoined to the ether solution and stirred for 2 h, the newly formed solid was filtered. Drying of the solid product obtained 1.00 g of the salt. Sodium (4-(*tert*-butyl)−1,2-phenylene)dimethanolate is soluble in water, dimethylsulfoxide (DMSO) and dimethylformamide (DMF). Yield: 1.00 g (84.00%). Melting point: 300 °C.

2.2. Synthesis of 4,4′-(((4-(tert-butyl)−1,2-phenylene) bis(methylene))bis(oxy))diphthalo-nitrile (1)

1.52 g (12.6 mmol) 4-nitrophthalonitrile, 1.00 g (4.4 mmol) sodium (4-(*tert*-butyl)−1,2-phenylene)dimethanolate, 5.34 g (50 mmol) anhydrous sodium carbonate and 20 mL dry DMF heated at 55 °C for 24 h and the compound of 4,4′-(((4-(*tert*-butyl)−1,2-phenylene)- bis(oxy))bis(methylene))diphthalonitrile was obtained by nucleophilic aromatic substitution reaction. The crude product was precipitated by a reaction mixture poured into the water and after it was filtered and dried, the raw product was purified via column chromatography eluting with $CHCl_3$. The structure of the substance was elucidated through elemental analysis, FT-IR, ^{1}H-NMR, and ^{13}C-NMR.

Complex 1 is soluble in dichloromethane (DCM), tetrahydrofuran (THF), $CHCl_3$, acetonitrile, acetone, DMSO, and DMF. Yield: 1.57 g (35.71%). Melting point: 188 °C. Elemental Analysis of $C_{28}H_{22}O_2N_4$ calculated: C, 75.32; H, 4.97; N, 12.55, obtained results: C, 75.15; H, 5.11; N, 12.67. IR (KBr pellet) ν_{max}/cm^{-1}: 3116.74(Ar-H), 3047.71(Ar-H), 2966.72(Alp-H), 2232.80(C≡N), 1594.56(C=C), 1561.78(C=C), 1493.40, 1460.55, 1416.38, 1387.65, 1364.81, 1306.17(Ar-O-Ar), 1297.04(Ar-O-Ar), 1249.59(Ar-O-Ar), 1205.28, 1177.90, 1104.51, 1093.17, 1082.71, 1032.77, 983.11, 944.13, 928.50, 882.88, 870.11, 843.81, 831.46, 758.38, 711.42, 642.32, 625.20, 605.97, 521.73, 456.64. ^{1}H-NMR data ($CDCl_3$) ppm: 1.36(s, 9H), 5.24(s, 2H), 5.25(s, 2H), 7.25(d, *J*=8.81 Hz, 1H), 7.30(d, *J*=8.81 Hz, 1H), 7.33(s, 1H), 7.36(s, 1H), 7.43(d, *J*=8.00 Hz, 1H), 7.51(s, 1H), 7.51(s, 1H), 7.73(d, *J*=8.00 Hz, 1H), 7.76(d, *J*=8.00 Hz, 1H). ^{13}C-NMR ppm: 31.18(3C), 34.82, 68.83, 69.53, 108.06, 115.04, 115.08, 115.36, 117.68, 119.47(2C), 119.78(2C), 119.81(2C), 126.76(2C), 127.33(2C), 129.78, 130.08, 132.43, 135.31(2C), 153.18, 161.33.

2.3. Synthesis of mononuclear (5-(tert-butyl)−2-((3,4-dicyanophenoxy)methyl)phenyl)-methanolate substituted metallo phthalocyanines (CoPc (2), Fe(OAc)Pc (3), Mn(OAc)Pc (4), NiPc (5), ZnPc (6))

100 mg (0.22 mmol) 4,4′-(((4-(*tert*-butyl)−1,2-phenylene)bis (methylene))bis(oxy))diphthalonitrile starting compound, 0.06 mmol metal salt, 12 mg (0.22 mmol) sodium methoxide and 0.25 mL DBU as catalyst and 0.25 mL dry DMF. It was refluxed for 12 h in an inert medium (N_2 atmosphere). After the system was cooled, the reaction concoction was diluted with DMF and the Pc was precipitated by adding acetic acid-water (7/3). The crude mono-nuclear Pc compound was washed with acetic acid-water (7/3) mixture, water, and methanol, respectively, by using the Soxhlet tool and then was dried. (Except for Fe(OAc)Pc and Mn(OAc)Pc; in these Pc species methanol was used instead of acetic acid) Molecular structures of Pc complexes were elucidated with elemental analyses, UV-Vis, FT-IR and MALDI-TOF-MS. It was observed that the MPcs dissolved in chloroform, DCM, THF, DMF, DMSO, and toluene at room temperature.

For CoPc (2) Yield: 60 mg (58.06%). Melting point >300 °C. Elemental Analysis of $C_{112}H_{88}CoN_{16}O_8$ calculated: C,72.91; H,4.81; N, 12.15, obtained results: C,73.07; H,4.65; N, 12.26. UV-*vis* data (λ_{max} nm (A)) 350(1.434), 622(0.700), 683(0.992) (Solvent: $CHCl_3$, M:1×10^{-6} molar). FT-IR data (KBr pellet)ν_{max}/cm^{-1}: 3058.99(Ar-H), 2955.39(Alp-H), 2923.50(Alp-H), 2863.30(Alp-H), 2227.33(C≡N), 1607.35(C=C), 1522.63, 1462.27, 1479.49, 1463.04, 1404.73, 1361.99(Ar-O-Ar), 1260.94(Ar-O-Ar), 1228.03(Ar-O-Ar), 1121.47, 1096.19, 1062.52, 1005.48, 879.91, 822.13, 751.36, 661.36, 605.75. MALDI-TOF-MS data (M/z):1687.867(M-CH_2O-phthalonitrile)$^+$, 1789.889(M-t-butyl)$^+$, 1847.547 (M+2H)$^+$.

For Fe(OAc)Pc (3) Yield: 26 mg (24.40%). Melting point >300 °C. Elemental Analysis of $C_{114}H_{91}FeN_{16}O_{10}$ calculated: C,72.03; H, 4.83; N, 11.79, obtained results: C,72.12; H, 4.97; N, 11.95. UV-*vis* data (λ_{max} nm (A)) 360(1.941), 607(0.431), 710(1.024) (Solvent: $CHCl_3$, M:1×10^{-6} molar). FT-IR data (KBr pellet)ν_{max}/cm^{-1}: 3059.65(Ar-H), 2951.70(Alp-H), 2924.55(Alp-H), 2857.95(Alp-H), 2224.43(C≡N), 1709.28(C=O), 1607.05(C=C), 1500.31, 1459.69, 1393.04, 1363.26,

1259.74(Ar-O-Ar), 1220.03(Ar-O-Ar), 1200.52(Ar-O-Ar), 1123.60, 1083.89, 1022.91, 925.06, 888.19, 822.19, 752.05, 621.59, 579.04. MALDI/TOF/MS data (M/ z): 1842.867 $(M\text{-}OAc+H)^+$.

For Mn(OAc)Pc (4) Yield: 40 mg (37.46%). Melting point >300 °C. Elemental Analysis of $C_{114}H_{91}MnN_{16}O_{10}$ calculated: C, 72.07; H,4.83; N,11.80, obtained results: C, 71.92; H, 4.95; N, 11.62. UV-*vis* data (λ_{max} nm (A)) 372(0.862), 523(0.204), 671(0.334), 737(0.636) (Solvent: $CHCl_3$, M:1×10^{-6} molar). FT-IR data (KBr pellet)ν_{max}/cm^{-1}: 3074.27(Ar-H), 2955.43(Alp-H), 2920.40(Alp-H), 2852.06(Alp-H), 2228.51(C≡N), 1717.72(C=O), 1596.37 (C=C), 1562.72, 1460.09, 1377.18, 1338.16(Ar-O-Ar), 1321.11(Ar-O-Ar), 1241.02(Ar-O-Ar), 1086.69, 1054.53, 995.03, 886.55, 828.68, 746.90, 730.28, 662.62, 616.53, 522.83, 453.32, 406.96. MALDI-TOF-MS data (M/z): 1840.373$(M\text{-}OAc)^+$, 1857.754$(M\text{-}OAc +H_2O)^+$, 1874.942 $(M\text{-}OAc +2H_2O)^+$.

For NiPc (5) Yield: 31 mg (29.98%). Melting point >300 °C. Elemental Analysis of $C_{112}H_{88}NiN_{16}O_8$ calculated: C,72.92; H,4.81; N, 12.15, obtained results: C,73.07; H,4.99; N, 12.08. UV-*vis* data (λ_{max} nm (A)) 386(1.121), 626(0.949), 678 (0.950) (Solvent: $CHCl_3$, M:1×10^{-6} molar). FT-IR data (KBr pellet)ν_{max}/cm^{-1}: 3060.82(Ar-H), 2959.13(Alp-H), 2930.69(Alp-H), 2868.45(Alp-H), 2223.47(C≡N), 1612.38(C=C), 1531.32, 1479.63, 1414.16, 1385.92, 1363.34, 1323.81(Ar-O-Ar), 1228.11(Ar-O-Ar), 1124.77, 1095.05, 1065.48, 1020.30, 867.61, 828.32,752.01. MALDI/TOF/MS data (M/z):1815.586$(M\text{-}2CH_3+H)^+$.

For ZnPc (6) Yield: 60 mg (57.82%). Melting point >300 °C. Elemental Analysis of $C_{112}H_{88}ZnN_{16}O_8$ calculated: C,72.66; H,4.79; N, 12.10, obtained results: C, 72.49; H,4.62; N,11.92. UV- *vis* data (λ_{max} nm (A)) 347(0.808), 621(0.226), 686(0.636) (Solvent: $CHCl_3$, M:1×10^{-6} molar). FT-IR data (KBr pellet)ν_{max}/cm^{-1}: 3060.47(Ar-H), 2956.39(Alp-H), 2922.78(Alp-H), 2852.32(Alp-H), 2222.22(C≡N), 1605.53(C=C), 1523.61, 1482.68, 1460.38, 1394.33, 1362.01, 1339.52(Ar-O-Ar), 1260.83(Ar-O-Ar), 1222.82(Ar-O-Ar), 1089.18, 1046.11, 999.49, 941.84, 872.94, 823.13, 773.20, 746.23, 728.24, 659.38, 521.66. MALDI-TOF-MS data (*M/z*): 1815.586$(M\text{-}CN\text{-}CH_3+2H)^+$, 1851.453$(M)^+$.

2.4. Electrochemical measurements

Electrochemical redox behaviors of novel Pc complexes were attentively examined by using SWV, CV, CPC, *in-situ* Spectroelectrochemical, and *in-situ* electrocolorimetric techniques at 25°C. In all electrochemical and spectroelectrochemical surveys, a three-electrode system was utilized. A platinum working electrode with a covering field of 0.10 cm^2 was used in electrochemical measurements. A spiral platinum wire was utilized being the counter electrode. The saturated calomel electrode (SCE) was utilized being the reference electrode. A bridge was used to separate the SCE from the solution. During the cyclic and square wave voltammetry surveys, which were achieved with Gamry Reference 600 Model galvanostat or potentiostat, pure nitrogen gas was passed through the solutions for 30 min. The solutions were kept in an atmosphere of inert nitrogen gas for the duration of the experiments. CV and SWV techniques were supported by *in situ* spectroelectrochemistry. Spectroelectrochemical redox behaviors were monitored via the diode array UV–Vis spectrophotometer named Ocean Optics HR2000+ operating in combination with Gamry Reference 600 potentiostat/galvanostat during the potentiostatic control. A thin layer spectroelectrochemical cell manufactured using a quartz cuvette and the three electrodes format were utilized to achieve the spectroelectrochemical measurements at 25°C. In this system, a translucent and wire mesh platinum gauze working electrode, a spiral platinum wire counter electrode, and a saturated calomel reference electrode (SCE) were operated [35].

3. Results and discussion

3.1. Synthesis and characterizations

Firstly, the diol compound (4-(tert-butyl)−1,2-phenylene) dimethanol) was obtained by reducing 4-*tert*-butylphthalic anhydride with $LiAlH_4$ in one step by conventional method [34]. Then, 4-(tert-butyl)−1,2-phenylene)dimethanol was converted into its salt, which is a stronger nucleophile, by reacting with the very strong base $NaNH_2$. Finally, starting compound 4,4′-(((4-(tert-butyl)−1,2-phenylene)bis(methylene))bis(oxy))diphthalonitrile (1) was obtained nucleophilic aromatic substitution reaction between 4-nitrophthalonitrile and sodium salt of 4-(tert-butyl)−1,2-phenylene)dimethanol. This compound was purified, and characterized by elemental analyses, FT-IR, UV–*Vis*, ^{1}H- and ^{13}C-NMR spectra. In the FT-IR spectrum of the 4,4′-(((4-(tert-butyl)−1,2-phenylene)bis(methylene))bis(oxy))diphthalonitrile, bands in the range of 3116.74–3047.71 cm^{-1} and 2966.72–2850.00 cm^{-1} show the stretching vibrations of the aromatic CH bonds (in the rings of aromatic benzene) and aliphatic CH bonds (in the tertiary butyl group and -CH_2 groups on the bridge), respectively. The stretching vibration of the C≡N bond was monitored at 2232.80 cm^{-1} and that of the C=C bond in benzene rings was monitored between 1594.56 and 1561.78 cm^{-1}. The bands seen in the range of 1306.17–1249.59 cm^{-1} belong to the stretching vibrations of the carbon-oxygen bonds in the (-CH_2-O-Ar) group. The presence of bands of the -CH_2-O-Ar and C≡N bonds is a strong indication of the formation of the target compound.

The ^{13}C-NMR and ^{1}H-NMR spectra of the 4,4′-(((4-(tert-butyl)−1,2-phenylene)bis-(methylene))bis(oxy))diphthalonitrile exactly match the proposed molecular construction. The molecular structure of starting materials was confirmed by the singlets at 1.36, 5.24, and 5.25 ppm in the aliphatic region and singlets and doublets in the range of 7.33–7.76 ppm in the ring with electron-withdrawing nitrile groups and in the range of 7.25–7.36 ppm in the ring with electron-releasing t-butyl group in the aromatic region. A detailed description of the ^{1}H-NMR and ^{13}C-NMR spectra of compound 1 is shown on the molecules in Fig. S1 and Fig. S2.

All the bands in the FT-IR spectra of the Pc molecules were generally similar to those in the FT-IR spectrum of compound 1. However, an extra peak around 1700 cm^{-1} was observed in the spectra of FePc and MnPc. This peak should belong to the C=O bond in the acetate group attached to the Pc ring from the axial position, pointing out that the formulas of these Pc complexes are Fe(OAc)Pc (3) and Mn(OAc)Pc (4), and the oxidation number of the metals is +3 (Fig. S3).

In general, the MALDI-TOF mass spectra of the Pc compounds well confirmed their molecular structures (Figs. S4-S8). Unfortunately, the molecular ion (M^+) peaks of the Pc molecules were not observed in most of their MALDI-TOF mass spectra. This situation occurred most probably due to the fact that the Pc molecules could not be ionized easily by laser light and thus, degradation products of the Pc molecules formed under these conditions despite the ionization assistance of the matrix molecule. The $(M\text{-}OAc)^+$ peak has been observed as the main one in the mass spectra of Fe(OAc)Pc (3) and Mn(OAc)Pc (4) complexes since the acetate group in the axial position in the molecules of these compounds is easily split by the laser light effect.

The -CH_2O- bridge in the structure of the Pc compounds in this study presents less mesomeric electron current and more inductive electron current than the classical oxo bridge. In this work, according to the Q bands of classical oxo bridged Pcs, red shifting was observed in the Q bands of CoPc (2), NiPc (5), and ZnPc (6) while blue shifting in those of Fe(OAc)Pc (3) and Mn(OAc)Pc (4). This situation shows that inductive electron current is more effective in the -OCH_2- bridge. However, unexpected results for Fe(OAc)Pc

(3) and Mn(OAc)Pc (4) can be explained that the electronic effects of the axially linked substituents (electron withdrawing acetate group) are stronger than electron releasing effect of -OCH_2- group.

The aggregation is generally unavoidable for Pc molecules due to their high molecular mass and unfortunately, it is often a major disadvantage for various technological applications. Unluckily, the novel molecules which contain four branched substituents in this study have high molecular weight and thus, most probably form aggregated species in solution. However, to prevent these compounds from aggregation, t-butyl groups have been included as substituents so that increase solubility and decrease aggregated species in common solvents. Therefore, it was thought that H aggregates formed by face-to-face interaction in solutions of CoPc (2) and NiPc (5) are examples. In the UV-*vis* spectrum of the Pcs except for Mn(OAc)Pc (4) and ZnPc (6), the extra bands were monitored between the vibrational bands and Q bands. These bands may originate from H aggregates formed by face-to-face interaction in solutions of CoPc (2) and NiPc (5). In fact, since the absorbance of the extra band of NiPc (5) is higher than that of CoPc (2), it can be stated that there are more H aggregated species in the NiPc (5) solution. Due to the variable valence of the metals in FePc and MnPc and their higher coordination numbers compared to other metals, the spectral behaviors of these two complexes are different [36,37]. UV-*vis* spectra of complexes Fe(OAc)Pc (3) and Mn(OAc)Pc (4) in DMSO solution showed that Fe(OAc)Pc (3) has a mixture of FePc and Fe(OAc)Pc species, whereas Mn(OAc)Pc (4) has only Mn(OAc)Pc species. When the absorbance values of the bands were compared for the Fe complex Fe(OAc)Pc (3), it was observed that it was predominantly Fe(OAc)Pc species in the DMSO solution (Fig. S9). This result do not show that these compounds are not pure, it show that these pure species formed the mixture of M+2 and M+3 of Pcs in DMSO.

3.2. *Electrochemistry and* in situ *spectroelectrochemistry*

It is exhibited by controlled potential coulometric investigations that redox processes thoroughly analyzed for Pc complexes broadly cover the transfer of one electron [38]. Characteristic data of complexes of redox processes, such as reduction and oxidation half-peak potentials ($E_{1/2}$), anodic-cathodic peak potential divisions ((ΔE_p), peak currents ratio (I_{pa}/I_{pc}), and initial oxidation-initial reduction half-peak potential differences were determined by using a carrier electrolyte in 0.10 mole dm^{-3} concentration, tetrabutylammoniumperchlorate (TBAP) salt, in absolutely pure DCM and DMSO solvent media. Voltammetric data obtained from electrochemical definitions are summarized in Table 1. It has been sighted that complexes usually form redox peaks with one electron transfer per redox-active species, arising from metals and/or Pc ligands. The ΔE_p values, varying in the range of 60–90 mV with 0.100 V s^{-1} scan rate, and the peak currents ratio, having unit value, of all redox processes in both solvent mediums reveal that these processes are reversible events with one electron transfer for MPc complexes [39]. This electrochemical reversibility was also strongly supported by the fact that the peak currents change in direct proportion to the square root of the potential scanning speed for cyclic voltammograms recorded at different scan rates. In addition, this reversibility displayed that chemical reactions do not accompany electron transfer processes as a result of voltammograms recorded at different scan rates. The reversible character of electrochemical reactions supports that compounds can transfer electrons rapidly. Therefore, it is possible to attribute the rapid occurrence of electron transfer to the high conjugation in compounds. The peak symmetry of the forward and backward SWV scans also props reversibility conditions from CV.

The metal centers, solvent environment, and environmental conditions of the complexes change the electrochemical parameters. For this reason, when consistent similarities in general redox behaviors of metal Pcs are attentively examined; it is understood that the conducts of NiPc (5) and ZnPc (6) complexes are exactly similar to each other and that CoPc (2), Fe(OAc)Pc (3), and Mn(OAc)Pc (4) compounds own quite analogous redox properties among themselves. These results, which are based on NiPc (5) and ZnPc (6) complexes, demonstrate that they behave as having an inactive metal center; all events happened like as in the form of two consecutive reductions and one or two oxidations centered on the Pc ring and also the third reduction centered on nitrile groups located at four peripheral corner tails of the Pc complex [23]. However, the redox attitudes CoPc (2), Fe(OAc)Pc (3), and Mn(OAc)Pc (4) compounds are remarkably different from that of NiPc (5) and ZnPc (6) complexes. This other way of behaving can be explained by the redox-active metal centers in the CoPc (2), Fe(OAc)Pc (3), and Mn(OAc)Pc (4) compounds. Therefore, these complexes have both ring-centered and metal-centered electron transfer transactions because they have redox active metals in the ring centers. The main molecular reason for this voltammetric difference is that complexes with electro-active metals such as CoPc (2), Fe(OAc)Pc (3), and Mn(OAc)Pc (4) own various half-filled and/or empty d orbitals between the lowest unoccupied molecular orbital (LUMO) and the highest occupied molecular orbital (HOMO). Consequently, while the first reduction events of CoPc (2), Fe(OAc)Pc (3), and Mn(OAc)Pc (4) compounds take place at pretty low negative potential values meaning closer to zero, their first oxidation takes place at lower positive potentials, compared to NiPc (5) and ZnPc (6) (Table 1). Complexes with such rich and low potential redox behavior generally have the capacity to own higher electrocatalytic activity, and elucidation of electrochemical redox actions is of great importance in this respect. The axial position occupied by the coordination property of neutralizing and/or donor solvent molecule significantly affects the potential of redox processes of MPcs. In order to make a comparison, it can be seen that in the Pc complexes, manganese and iron can have an oxidation state of +3, while cobalt metal has a state of +2. Therefore, the acetate ion is bound from the axial position to the Fe(OAc)Pc (3) and Mn(OAc)Pc (4) compounds; moreover, for CoPc (2) complex, donor DMSO solvent binding takes place from the axial position. *In situ* spectral and IR spectroscopy characterizations made this situation more evident. In IR spectroscopy, the carbonyl peak was observed due to the binding of the acetate group to the Mn(OAc)Pc (4) complex, and therefore it was understood that before the redox reactions, the original state of manganese metal in the complex was in the Mn (III) valence state. In addition, iron metal had the same behavior as manganese metal. However, cobalt metal in the original state had an oxidation state of +2. The initial reduction and oxidation events of complexes with redox active metal centers in polar solvents as in as DMSO and DMF happen on the metal center. On the other hand, the initial oxidation which happens in an apolar solvent such as DCM belongs to the Pc ring.

SWV and CV voltammograms for CoPc (2) in the DMSO-TBAP solution medium are represented in Fig. 1. Furthermore, it can be noticed in Table 1 and Fig. 1 that CoPc (2) showed two oxidation attitudes with one electron. The first oxidation redox process for cobalt metal specified O1 at 0.42 V of $E_{1/2}$ value can be ascribed to the redox couple Co(II)Pc(−2)/[Co(III)Pc(−2)]$^+$. The secondary oxidation process, which was characterized by O2 at 1.04 V half-wave potential, is in the form of [Co(III)Pc(−2)]$^+$/[Co(III)Pc(−1)]$^{2+}$ and belongs to the Pc ring. Moreover, the CoPc (2) complex showed three reduction processes with one-electron (−0.50 V for R1, −1.43 V for R2, and −1.57 V for R3 *versus* SCE) [40]. The first reduction redox process defined R1, Co(II)Pc(−2)/[Co(I)Pc(−2)]$^-$, obviously demonstrating the electron transfer of the cobalt

Table 1
The electrochemical redox data for CoPc (2), Fe(OAc)Pc (3), Mn(OAc)Pc (4), NiPc (5) and ZnPc (6) corresponding to previous studies.

Complexes	Redox Processes	Process	[a]$E_{1/2}$(V)	[b]ΔE_p(mV)	[c]I_{pa}/I_{pc} (V)	[d]$\Delta E_{1/2}$ (V)	Refs.
CoPc (2) (in DMSO)	$[Co(III)Pc(-2)]^+/[Co(III)Pc(-1)]^{2+}$	[e] O2	1.04	–	–	0.92	[38]
	$Co(II)Pc(-2)/[Co(III)Pc(-2)]^+$	O1	0.42	80	0.80		
	$Co(II)Pc(-2)/[Co(I)Pc(-2)]^-$	R1	−0.50	65	0.85		
	$[Co(I)Pc(-2)]^-/[Co(I)Pc(-3)]^{2-}$	[e] R2	−1.43	–	–		
	Nitrile Reduction	[e] R3	−1.57	–	–		
Fe(OAc)Pc (3) (in DMSO)	$[Fe(IV)(OAc)Pc(-2)]^+/[Fe(IV)(OAc)Pc(-1)]^{2+}$	[e] O2	1.09	–	–	0.50	[30]
	$Fe(III)(OAc)Pc(-2)/[Fe(IV)(OAc)Pc(-2)]^+$	O1	0.15	70	0.88		
	$Fe(III)(OAc)Pc(-2)/[Fe(II)(OAc)Pc(-2)]^-$	R1	−0.35	60	0.95		
	$[Fe(II)(OAc)Pc(-2)]^-/[Fe(I)(OAc)Pc(-2)]^{2-}$	[e] R2	−1.08	–	–		
	$[Fe(I)(OAc)Pc(-2)]^{2-}/[Fe(I)(OAc)Pc(-3)]^{3-}$	[e] R3	−1.36	–	–		
	Nitrile Reduction	[e] R4	−1.60	–	–		
Mn(OAc)Pc (4) (in DMSO)	$Mn(IV)(OAc)Pc(-2)^+/[Mn(IV)(OAc)Pc(-1)]^{2+}$	[e] O2	1.00	–	–	0.68	[31]
	$Mn(III)(OAc)Pc(-2)/[Mn(IV)(OAc)Pc(-2)]^+$	O1	0.39	90	0.80		
	$Mn(III)(OAc)Pc(-2)/[Mn(II)(OAc)Pc(-2)]^-$	R1	−0.29	75	0.85		
	$[Mn(II)(OAc)Pc(-2)]^-/[Mn(I)(OAc)Pc(-2)]^{2-}$	R2	−0.90	85	0.88		
	$[Mn(I)(OAc)Pc(-2)]^{2-}/[Mn(I)(OAc)Pc(-3)]^{3-}$	R3	−1.30	80	0.85		
	$[Mn(I)(OAc)Pc(-3)]^{3-}/[Mn(I)(OAc)Pc(-4)]^{4-}$	[e] R4	−1.54	–	–		
	Nitrile Reduction	[e] R5	−1.70	–	–		
NiPc (5) (in DMSO)	$Ni(II)Pc(-2)/[Ni(II)Pc(-1)]^+$	[e] O1	0.97	–	–	1.54	[45]
	$Ni(II)Pc(-2)/[Ni(II)Pc(-3)]^-$	R1	−0.57	80	0.75		
	$[Ni(II)Pc(-3)]^-/[Ni(II)Pc(-4)]^{2-}$	[e] R2	−1.02	–	–		
	Nitrile Reduction	[e] R3	−1.40	–	–		
ZnPc (6) (in DMSO)	$[Zn(II)Pc(-1)]^+/[Zn(II)Pc(0)]^{2+}$	[e] O2	1.00	–	–	1.55	[31]
	$Zn(II)Pc(-2)/[Zn(II)Pc(-1)]^+$	[e] O1	0.60	–	–		
	$Zn(II)Pc(-2)/[Zn(II)Pc(-3)]^-$	R1	−0.95	75	0.80		
	$[Zn(II)Pc(-3)]^-/[Zn(II)Pc(-4)]^{2-}$	[e] R2	−1.35	–	–		
	Nitrile Reduction	–	–	–	–		
ZnPc (6) (in DCM)	$Zn(II)Pc(-2)/[Zn(II)Pc(-1)]^+$	[e] O1	0.55	–	–	1.23	[38]
	$Zn(II)Pc(-2)/[Zn(II)Pc(-3)]^-$	[e] R1′	−0.68	–	–		
		[e](R1″)	(−0.92)				
	$[Zn(II)Pc(-3)]^-/[Zn(II)Pc(-4)]^{2-}$	[e] R2	−1.34	–	–		
	Nitrile Reduction	[e] R3	−1.68	–	–		

[a]: $E_{1/2} = (E_{pa} + E_{pc})/2$ at 0.100 V s^{-1} scan rate.
[b]: $\Delta E_p = E_{pa} - E_{pc}$ at 0.100 V s^{-1} scan rate.
[c]: I_{pa}/I_{pc}, at 0.100 V s^{-1} scan rate.
[d]: $\Delta E_{1/2}$ = $E_{1/2}$(first oxidation) - $E_{1/2}$ (first reduction). It represents the HOMO-LUMO gap for Zn and Ni, but the charge transfer transitions for Fe, Mn, and Co involving redox active metal centers.
[e]: This redox couples were just determined by using Square Wave Voltammetry (SWV).

metal center. The second reduction redox process marked R2, $[Co(I)Pc(-2)]^-/[Co(I)Pc(-3)]^{2-}$, belongs to the Pc ring centered electron transfer [41]. The final reduction process tagged R3 is caused by the nitrile groups that are placed at four peripheral tails in the structure of the complex CoPc (2).

Cyclic and square wave voltammograms for Fe(OAc)Pc (3) in DMSO/TBAP environment are revealed in Fig. 2. Fe(OAc)Pc (3) complex; showed two oxidation and four reduction behaviors with one electron. $E_{1/2}$ value of 0.15 V for the first oxidation pair labeled O1 belongs to iron metal, which can be attributed to the redox pair, $Fe(III)(OAc)Pc(-2)/[Fe(IV)(OAc)Pc(-2)]^+$. The second oxidation process, $[Fe(IV)(OAc)Pc(-2)]^+/[Fe(IV)(OAc)Pc(-1)]^{2+}$, displayed by O2 labeled with 1.09 V half-wave potential, belongs to the Pc ring. Also, Fe(OAc)Pc (3) showed a series of four reduction behaviors. The first reduction event labeled R1 occurred at −0.35 V half-wave potential value. The R1 reduction redox pair, $Fe(III)(OAc)Pc(-2)/[Fe(II)(OAc)Pc(-2)]^-$, indicates the electron transfer of the iron metal center. The second reduction identified as R2, $[Fe(II)(OAc)Pc(-2)]^-/[Fe(I)(OAc)Pc(-2)]^{2-}$, was metal centered at −1.08 V half-wave potential value. The third reduction redox process labeled R3, $[Fe(I)(OAc)Pc(-2)]^{2-}/[Fe(I)(OAc)Pc(-3)]^{3-}$, took place at −1.36 V of $E_{1/2}$ value and belongs to Pc ring centered electron transfer [32]. The R4 redox process happening at −1.60 V half-wave potential belongs to the last reduction process due to the nitrile groups located at four peripheral corner tails of the Pc complex (Table 1 and Fig. 2). Additionally, the cause of the interplay betwixt Pc ligand molecular and Fe-d orbitals, the first ring centered reduction event for this complex occurs at a greatly negative potential (at −1.36 V). Thus, the second and ongoing ring-based reduction processes of Pc are often outside the range of current negative potential and unfortunately cannot be noticed as estimated. Additionally, when the charge transfer transition energies of CoPc (2), Fe(OAc)Pc (3), and Mn(OAc)Pc (4) compounds are compared in order of 0.92 V, 0.50 V, and 0.68 V, it can be observed from the Table 1 that the charge transfer transition energy for the complex Fe(OAc)Pc (3) is lower than the others.

In the solution medium that was prepared with pure DMSO and TBAP, CV and SWV voltammograms obtained for Mn(OAc)Pc (4) are displayed in Fig. 3. For this compound, two oxidations (0.39 V for O1 and 1.00 V for O2) and five reductions (−0.29 V for R1, −0.90 V for R2, −1.30 V for R3, −1.54 V for R4, and −1.70 V for R5) processes were noted with one electron transfer for each redox process [42]. The first reduction processes (R1), $Mn(III)(OAc)Pc(-2)/[Mn(II)(OAc)Pc(-2)]^-$ and the second one (R2), $[Mn(II)(OAc)Pc(-2)]^-/[Mn(I)(OAc)Pc(-2)]^{2-}$ for Mn(OAc)Pc (4) were metal centered (Table 1). The third reduction processes (R3), $[Mn(I)(OAc)Pc(-2)]^{2-}/[Mn(I)(OAc)Pc(-3)]^{3-}$ at −1.30 V and fourth reduction processes (R4), $[Mn(I)(OAc)Pc(-3)]^{3-}/[Mn(I)(OAc)Pc(-4)]^{4-}$ at −1.54 V belong to the ring of Pc rather than the reduction of manganese ions in the complex [43]. The R5 process at −1.70 V is the last reduction because of the nitrile groups located at four

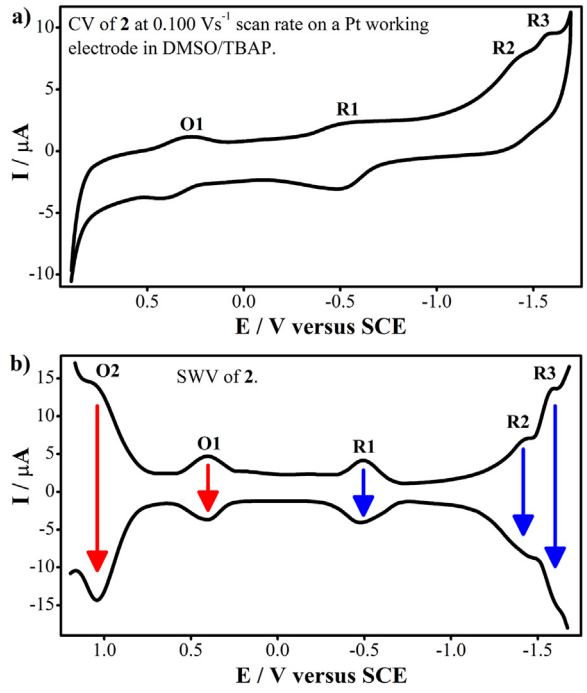

Fig. 1. (a) Cyclic voltammogram at 0.100 Vs^{-1} scan rate and (b) square wave voltammograms (pulse size: 100 mV; step size: 5 mV; frequency: 25 Hz.) of CoPc (2) (5.00×10^{-4} M) on a Pt working electrode in DMSO/TBAP electrolyte system.

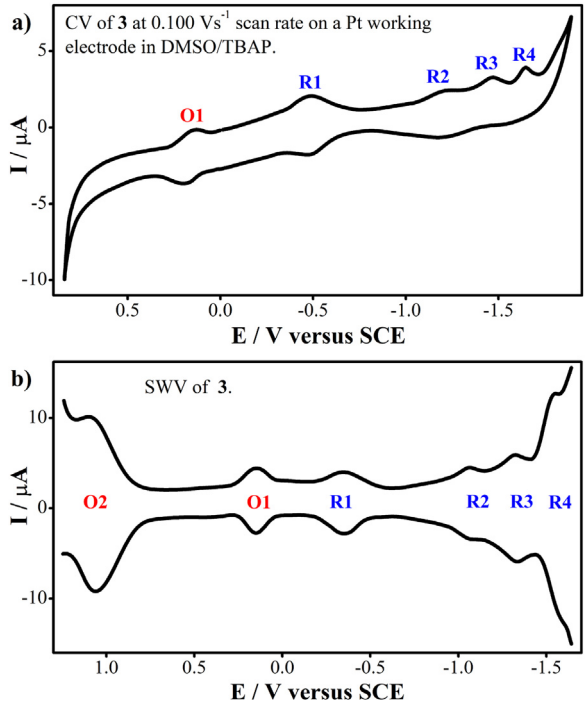

Fig. 2. (a) Cyclic voltammogram at 0.100 Vs^{-1} scan rate and (b) square wave voltammograms (pulse size: 100 mV; step size: 5 mV; frequency: 25 Hz.) of Fe(OAc)Pc (3) (5.00×10^{-4} M) on a Pt working electrode in DMSO/TBAP electrolyte system.

peripheral corner tails of the Pc structure. The initial oxidation reaction of Mn(OAc)Pc (4), obviously characterized as O1, Mn(III)(OAc)Pc(−2)/[Mn(IV)(OAc)Pc(−2)]$^{+}$ at 0.39 V is metal centered (Table 1). On the other hand, the first oxidation of the Pc ring is observed at 1.00 V as the second oxidation of Mn(OAc)Pc (4) (O2), Mn(IV)(OAc)Pc(−2)$^{+}$/ [Mn(IV)(OAc)Pc(−1)]$^{2+}$ (Fig. 3) [44].

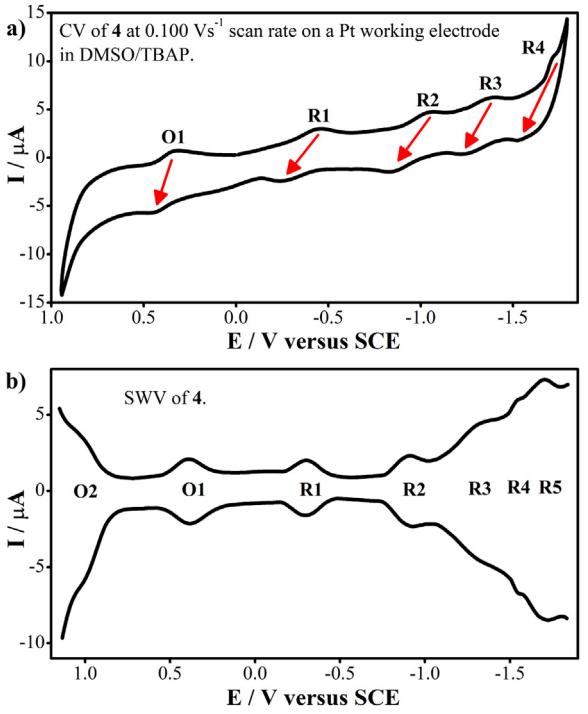

Fig. 3. (a) Cyclic voltammogram at 0.100 Vs^{-1} scan rate and (b) square wave voltammograms (pulse size: 100 mV; step size: 5 mV; frequency: 25 Hz.) of Mn(OAc)Pc (4) (5.00×10^{-4} M) on a Pt working electrode in DMSO/TBAP electrolyte system.

Generally, it is expected in the DMSO/TBAP electrolyte system that while the initial reduction and oxidation events of complexes containing redox-active metals such as Fe, Co, and Mn in the +2 valence state, are metal-centered corresponding to the [M(II)Pc(−2)]/[M(I)Pc(−2)]$^{-}$ and [M(II)Pc(−2)]/[M(III)Pc(−2)]$^{+}$ pairs, respectively, the second reduction belong to the Pc ring. Therefore, CoPc (2), Fe(OAc)Pc (3), and Mn(OAc)Pc (4) complexes containing redox active metal showed both ligand and metal originated electron transfer processes in voltammetric studies performed in a solution medium containing DMSO/TBAP and DCM/TBAP. For the CoPc (2), Fe(OAc)Pc (3), and Mn(OAc)Pc (4) complexes, valence states of redox active metals were determined as +3 for Mn and Fe, and +2 for Co by IR spectroscopy. Aimed at understanding this situation more clearly, these redox processes, metal or ligand centered, should be elucidated, which is possible by supporting voltammetric studies with *in situ* spectroelectrochemical analyzes. Therefore, *in situ* spectral changes of the complexes have been recorded at appropriate fixed potentials in order to support the redox behaviors. Additionally, *in situ* electrocolorimetric evaluations, which are a vital indicator for electrochromic applications by giving chromaticity (color) diagrams that allow the determination of x, y, and z coordinates, have been integrated into spectroelectrochemistry measurements.

In situ spectral and electrocolorimetric specifications of the Mn(OAc)Pc (4) complex are presented in Fig. 4, as an instance for the realization of the electron transfer behavior of redox-active metal-centered Pc complexes. All color changes involved in the redox processes were clearly and entirely given on the chromaticity diagram, also representing the color of the electrogenerated species in Fig. 4e. Additionally, Fig. 4a is obvious to grasp the oxidation state of the metal in Mn(OAc)Pc (4) before any potential is applied. The metal ligand charge transfer band (MLCT) remarked at 518 nm and the Q band at 745 nm confirm that the manganese species in the complex is in a +3 oxidation state initially. The spectral changes happening under −0.55 V constant potential *ver-*

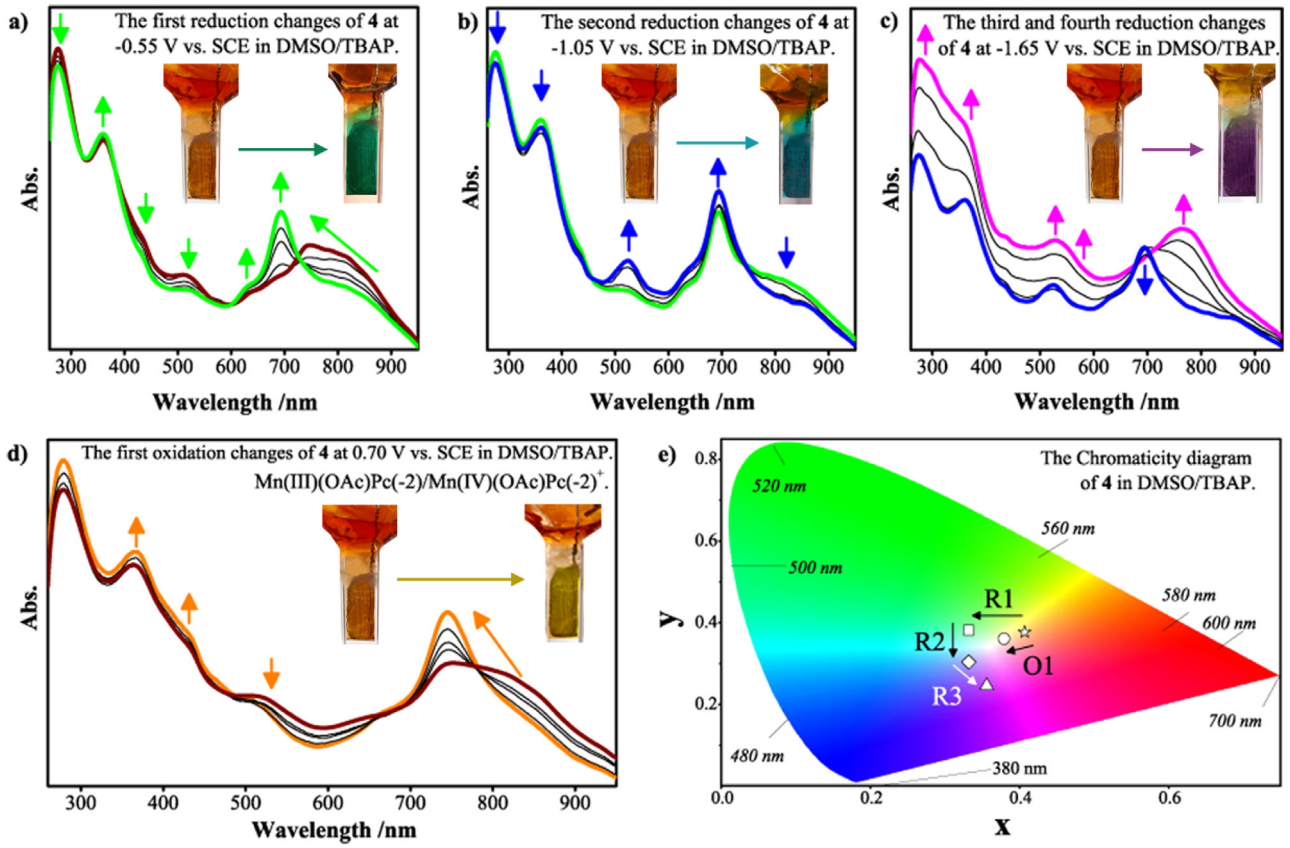

Fig. 4. *In situ* UV-vis spectral changes of Mn(OAc)Pc (4) during the controlled-potential electrolysis in DMSO/TBAP electrolyte system at (a) E_{app}= −0.55 V (b) E_{app}= −1.05 V (c) E_{app}= −1.65 V (d) E_{app}= 0.70 V (e) the chromaticity diagram with the color changes of Mn(OAc)Pc (4).

sus SCE in the DMSO/TBAP solution are given in Fig. 4a medium. For the R1 redox process, Mn(III)(OAc)Pc(−2)/[Mn(II)(OAc)Pc(−2)]$^{-}$, while the Q band shifts from 745 nm to 694 nm, new bands are recorded in the charge transfer zone. The existence of clear isosbestic points at 320, 382, and 600 nm obtained by analysis of the changes in the absorbance spectrum via UV–Vis spectrophotometer affirms the predominance of reduced [Mn(II)(OAc)Pc(−2)]$^{-}$ species. These changes point out the R1 tagged redox pair expressed by voltammetric measurements in Fig. 3. The color of the original spectrum, obtained by *in situ* color determination without applying any potential to the electrolyte, coincides with a burgundy-orange color in the color diagram in Fig. 4a which is indicated as the star token with position (x = 0.407, y = 0.377) on the chromaticity diagram fitted in the coordinate plane in Fig. 4e, before the first reduction process of the Mn(OAc)Pc (4). In the direction of reduction with the application of −0.55 V constant potential *versus* SCE, the reduction of the manganese metal Mn(III)(OAc)Pc(−2)/[Mn(II)(OAc)Pc(−2)]$^{-}$ starts, and during the R1 redox process initially observed burgundy-orange color turns into light green color as shown with square sign x = 0.332, y = 0.382 in Fig. 4a and 4e. In the second redox reduction process R2, [Mn(II)(OAc)Pc(−2)]$^{-}$/[Mn(I)(OAc)Pc(−2)]$^{2-}$, the changes in the absorbance spectrum recorded at −1.05 V can be seen in Fig. 4b. Notably, the composition of a novel band in the range of 500–550 nm in the MLCT transition region and the increase in the band indicate that the second reduction event is metal centered. In that case, the second reduction of manganese metal takes place in the way of Mn(II)/(Mn(I). At the end of the color investigations accompanying the second reduction of manganese metal R2 process [Mn(II)(OAc)Pc(−2)]$^{-}$/[M*n*(I)(OAc)Pc(−2)]$^{2-}$, the blue color is obtained in Fig. 4b (diamond symbol x = 0.332, y = 0.304). It can be noticed from Fig. 4c that while the magnitude of the Q band declines in the course of the R3 process under −1.65 V constant potential, the genesis of a clear peak at 765 nm, the increase in the peak intensity at 530 nm, and the formation of a wide band in this region indicate the Pc based reduction process. Besides, these changes in the absorbance spectrum are the characteristic behaviors of the Pc ligand centered reduction reactions [45]. Since the constant potential value of −1.65 V includes both R3 and R4 Pc reduction reactions, which were determined by using electrochemical techniques (Fig. 3 and Table 1). These changes corresponds to processes R3 [Mn(I)(OAc)Pc(−2)]$^{2-}$/[Mn(I)(OAc)Pc(−3)]$^{3-}$ and R4 [Mn(I)(OAc)Pc(−3)]$^{3-}$/[Mn(I)(OAc)Pc(−4)]$^{4-}$. With the constant potential −1,65 V, the total Pc reduction process, specified R3 on the chromaticity diagram produced the light pink color as shown with triangle sign x = 0.356, y = 0.246 in Fig. 4e. The changes in the absorbance spectrum via *in situ* UV–Vis spectrophotometer under the 0.70 V constant potential are presented in Fig. 4d. The same spectral properties of the original spectral wave seen in Fig. 4a obtained before both reduction and oxidation processes without applying any constant potential. In the beginning, the presence of the broad Q band between 714 and 850 nm and the 518 nm band demonstrates the existence of [Mn(III)(OAc)Pc(−2)]. These results confirm that the manganese ion in the Mn(OAc)Pc (4) complex is in the +3 oxidation state. The growth of the Q band and shifting to 745 nm indicates that there is metal-based oxidation. This oxidation process, O1, remarked via not only CV but also SWV, corresponds to Mn(III)(OAc)Pc(−2)/[M*n*(IV)(OAc)Pc(−2)]$^{+}$ (Fig. 3 and Table 1). During this electrolytic redox process, the increase strictly observed in the band of metal-ligand charge transfer region in the range of 440–480 nm reveals that O1 oxidation takes place on the metal and can be categorized as Mn(III)/Mn(IV)

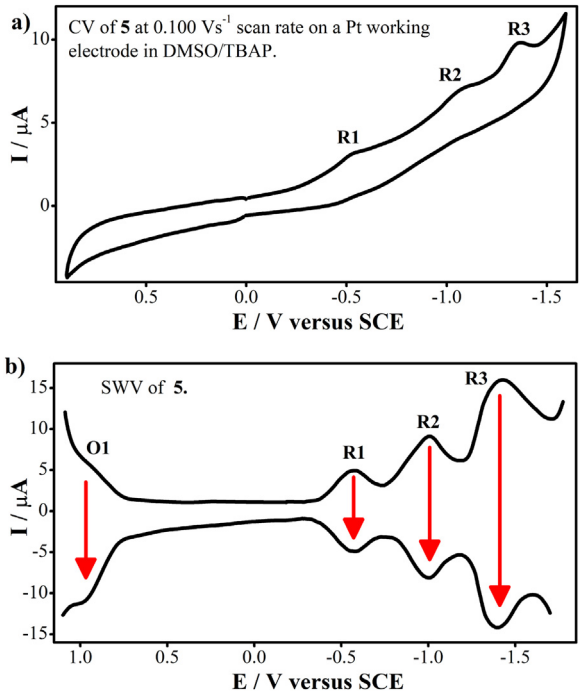

Fig. 5. (a) Cyclic voltammogram at 0.100 Vs^{-1} scan rate and (b) square wave voltammograms (pulse size: 100 mV; step size: 5 mV; frequency: 25 Hz.) of NiPc (5) (5.00×10^{-4} M) on a Pt working electrode in DMSO/TBAP electrolyte system.

[44]. As a result of the O1 oxidation of the manganese metal, Mn(III)(OAc)Pc(−2)/[M*n*(IV)(OA*c*)P*c*(−2)]$^{+}$, in the Pc complex under 0.70 V fixed potential, the burgundy-orange color changes to light yellow-light orange (circle sign $x = 0.379$, $y = 0.361$). Unfortunately, spectral changes corresponding to the oxidation event in the Pc ring and supporting CV and SWV characterizations could not be observed, probably due to the limited anodic working range of the DMSO/TBAP solution medium [46].

In this part of the study, it was tried to elucidate the differences in the basic redox act of complexes containing redox inactive nickel and zinc metal centers and understand the effect of these different metal centers on Pc centered redox events. Fig. 5 demonstrates SWV and CV voltammograms of complex NiPc (5) in DMSO/TBAP solution medium. In this complex, one electron oxidation, O1 at 0.97 V, Ni(II)Pc(−2)/[N*i*(II)P*c*(−1)]$^{+}$, and two one-electron reductions as R1 at −0.57 V for Ni(II)Pc(−2)/[N*i*(II)P*c*(−3)]$^{-}$ and R2 at −1.02 V for [Ni(II)Pc(−3)]$^{-}$/[N*i*(II)P*c*(−4)]$^{2-}$ were detected [47]. All redox processes occurred on the Pc ring, as the complex has redox inactive metal nickel, except R3, which is related to the nitrile groups attached to peripheral ends in the complex. The O1 oxidation process, which cannot be regrettably discovered with CV, was clearly determined by high precision square-wave voltammetry as highlighted in Fig. 5b [48].

Spectroelectrochemical and electrocolorimetric determinations, performed in order to clearly elucidate the electrochemical attitude of the NiPc (5) complex were detailed in Fig. 6. The colorimetric changes of the first oxidation and first reduction redox processes were given on the chromaticity diagram created by measuring the changes in the color of the redox-active compounds in Fig. 6c. Fig. 6a demonstrates the changes in the absorbance spectrum of the NiPc (5), under −1.20 V constant potential *versus* SCE in the medium containing the DMSO/TBAP solution medium. In the course of this redox process, the blue color of the original spectrum (star symbol $x = 0.292$, $y = 0.281$) turned into light purple color (square token $x = 0.350$, $y = 0.210$ as displayed in Fig. 6c). In this reduction process, which corresponds to the processes, R1 reduction Ni(II)Pc(−2)/[N*i*(II)P*c*(−3)]$^{-}$ and R2 reduction [Ni(II)Pc(−3)]$^{-}$/[N*i*(II)P*c*(−4)]$^{2-}$ (Table 1), while the magnitude of the Q band at 684 nm decreased with no shifting, the flatness band at 813 nm and the bands in the 460–600 nm region increased. The presence of well-defined isosbestic points at 284 nm and 718 nm during these changes in the absorbance spectrum corresponding to the R1 and R2 reduction processes of the Pc ring and the absence of moving isosbestic points are an indication of the electrochemical events occurring on a single species [47]. It can be plainly seen both in Fig. 6b and 6c, that before applying 1.10 V constant potential to the cell system, the color of the original spectrum was blue (star image $x = 0.292$, $y = 0.281$) and the initial spectrum was the same as the spectrum observed before first reduction process by *in situ* color measurement. Fig. 6b fully represents *in situ* spectroelectrochemical changes in the course of the first oxidation O1, Ni(II)Pc(−2)/[N*i*(II)P*c*(−1)]$^{+}$, of the Pc ring under constant 1.10 V potential. The increase in the band betwixt 500–600 nm interval, the decline in the magnitude of the Q band at 684 nm without shifting, and the increment in the flatness band at 815 nm between 780 nm and 900 nm indicate that the oxidation event is Pc based. After the first oxidation process of the NiPc (5) complex in the DMSO/TBAP electrolyte system, the beginning blue color converted to orange, which was symbolized with the circle token in the color diagram ($x = 0.432$ $y = 0.358$) in Fig. 6c.

Fig. 7 evidently represents the CV and SWV voltammograms of ZnPc (6) in the DMSO/TBAP solution medium. Two one-electron oxidation; Zn(II)Pc(−2)/[Z*n*(II)P*c*(−1)]$^{+}$ (O1), [Zn(II)Pc(−1)]$^{+}$/[Z*n*(II)P*c*(0)]$^{2+}$ (O2) and two one-electron reduction; Zn(II)Pc(−2)/[Z*n*(II)P*c*(−3)]$^{-}$ (R1) and [Zn(II)Pc(−3)]$^{-}$/[Z*n*(II)P*c*(−4)]$^{2-}$ (R2) processes occurring on the Pc ring, were noted for this complex [49]. Since zinc is a redox inactive metal, any redox process belonging to the metal that is centered in the core of the molecule of ZnPc (6), could not be detected [50]. Also, the reduction process of the nitrile groups was not detected. On the other hand, although the second oxidation process, [Zn(II)Pc(−1)]$^{+}$/[Z*n*(II)P*c*(0)]$^{2+}$ (O2) at 1.00 V, could not be monitored with CV, it was possible to determine it by SWV. Electrochemical data from this study clearly indicated that NiPc (5) and ZnPc (6) complexes act as redox inactive metal-centered complexes. This similarity in the redox nature of nickel and zinc phthalocyanine complexes is consistent with the studies in the literature (Table 1). As a consequence of this deduction, it has been understood that all redox processes originate from the Pc ring of the ZnPc (6) complex [51]. In addition, when the voltammetric nature of zinc metal-centered Pcs was thoroughly investigated, it was noticed that redox events occurred at slightly more negative potentials (O1 at 0.60 V, R1 at −0.95 V, and R2 at −1.35 V) for the complex ZnPc (6) than the nickel metal centered complex NiPc (5) (O1 at 0.97 V, R1 at −0.57 V and R2 at −1.02 V) in the DMSO/TBAP solution medium (Table 1). This can be attributed to the different polarization power of the atoms in the center.

The electrochemical characterization of ZnPc (6) including spectroelectrochemistry was also carried out in a solvent medium DCM/TBAP without coordinative properties. The results were quite similar to those obtained in DMSO/TBAP electrolyte system (Table 1). The SWV voltammogram of ZnPc (6) in the DCM/TBAP solution medium can be seen in Fig. 8. A one-electron oxidation at 0.55 V, Zn(II)Pc(−2)/[Z*n*(II)P*c*(−1)]$^{+}$ (O1) and two one-electron reductions were remarked for this complex. The first reduction R1, Zn(II)Pc(−2)/[Z*n*(II)P*c*(−3)]$^{-}$ was divided into two waves in SWV as R1′ at −0.68 V and R1″ at −0.92 V. To obviously reveal why the reduction of R1 split into two waves in SWV, *in situ* spectroelectrochemical analysis was performed. R2 reduction redox process, [Zn(II)Pc(−3)]$^{-}$/[Z*n*(II)P*c*(−4)]$^{2-}$, was certainly detected at −1.34 V via SWV. Since there is redox inactive zinc metal in the complex

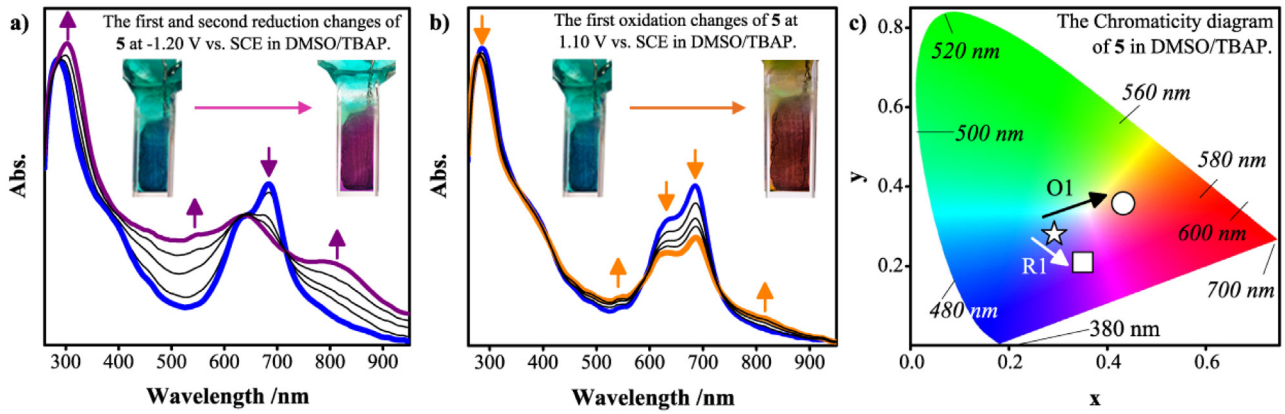

Fig. 6. *In situ* UV-vis spectral changes of NiPc (5) during the controlled-potential electrolysis in DMSO/TBAP electrolyte system at (a) E_{app}= −1.20 V (b) E_{app}= 1.10 V (c) the chromaticity diagram with the color changes of NiPc (5).

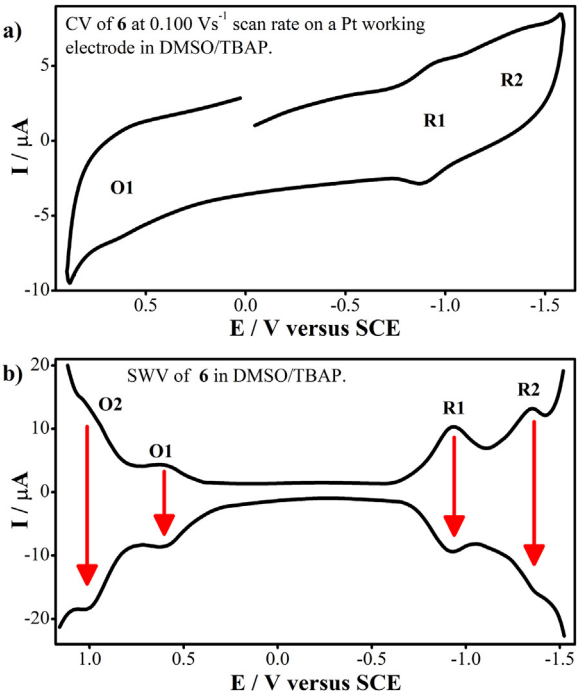

Fig. 7. (a) Cyclic voltammogram at 0.100 Vs^{-1} scan rate and (b) square wave voltammograms (pulse size: 100 mV; step size: 5 mV; frequency: 25 Hz.) of ZnPc (6) (5.00×10^{-4} M) on a Pt working electrode in DMSO/TBAP electrolyte system.

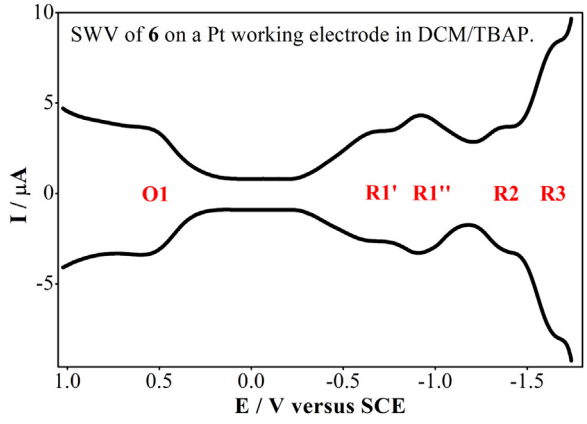

Fig. 8. Square wave voltammograms (pulse size: 100 mV; step size: 5 mV; frequency: 25 Hz.) of ZnPc (6) (5.00×10^{-4} M) on a Pt working electrode in DCM/TBAP electrolyte system.

center, the first two reduction and oxidation events took place on the Pc ring. Furthermore, in the DCM/TBAP system, the redox process R3 belonging to the nitrile groups located at peripheral tails of the Pc complex can be detected at −1.68 V since the operating range of the DCM/TBAP system shifts to more positive compared to the DMSO/TBAP electrolyte system.

In situ electrocolorimetric and spectroelectrochemical analyzes were also operated to elucidate the electrochemical redox conduct of the ZnPc (6) in DCM/TBAP solution (Fig. 9). As a result of the first oxidation and the first reduction redox processes, the colorimetric changes were given on the diagram of chromaticity in Fig. 9c. Before applying any constant potential for first reduction and oxidation processes, the same original spectrums were easily acquired with light blue color demonstrated by using star emblem (x = 0.282, y = 0.286) on the diagram of chromaticity in Fig. 9. The spectral changes of the ZnPc (6) complex under −1.20 V fixed potential in the medium containing the DCM/TBAP system were presented in Fig. 9a. In this reduction process, during the decline in the magnitude of the Q band at 688 nm with no shifting, it was noticed that the bands in the 460–600 nm region and the flatness band at 809 nm increased. Not only observations of the changing isosbestic points in the 600–660 nm and 700–800 nm regions in the time of the spectroelectrochemical R1 process of mononuclear zinc phthalocyanine complex, but also the splitting of the peak of the first reduction process defined R1 in SWV are indications and evidence of the presence of aggregation in this complex. This way of behaving is typical of mononuclear metal-centered phthalocyanine complexes [32]. When the changes in the absorbance spectrum of ZnPc (6) recorded via *in situ* UV-vis spectrophotometer are examined, the existing moving isosbestic points verify that the splitting of the peak of the R1 reduction process in SWV into R1′ and R1′′ is due to aggregation (Fig. 8 and Table 1). After applying −1.20 V constant potential, the light blue color of the complex in the DCM/TBAP electrolyte system turned into purple color marked by the square emblem, which can be simply shown on the chromaticity diagram together with coordinates x = 0.350, y = 0.240 in Fig. 9a and c. Furthermore, Fig. 9b expresses the *in situ* spectroelectrochemical changes in which oxidation O1, Zn(II)Pc(−2)/[Zn(II)Pc(−1)]$^{+}$, of the Pc ring is remarked at 0.80 V. Not only the upsurges in the band in the range of 500–600 nm and the planarity band between 780 nm and 900 nm at 814 nm but also decline in the magnitude of the 688 nm band with no shifting indicate that the oxidation redox process is Pc based. During the O1 process, the clear and well-defined isosbestic points, which were seen at 323 nm, 391 nm, 609 nm, and 728 nm in the spectroelectrochemical process of the ZnPc (6) complex, demonstrate that the oxidation event happened on a single

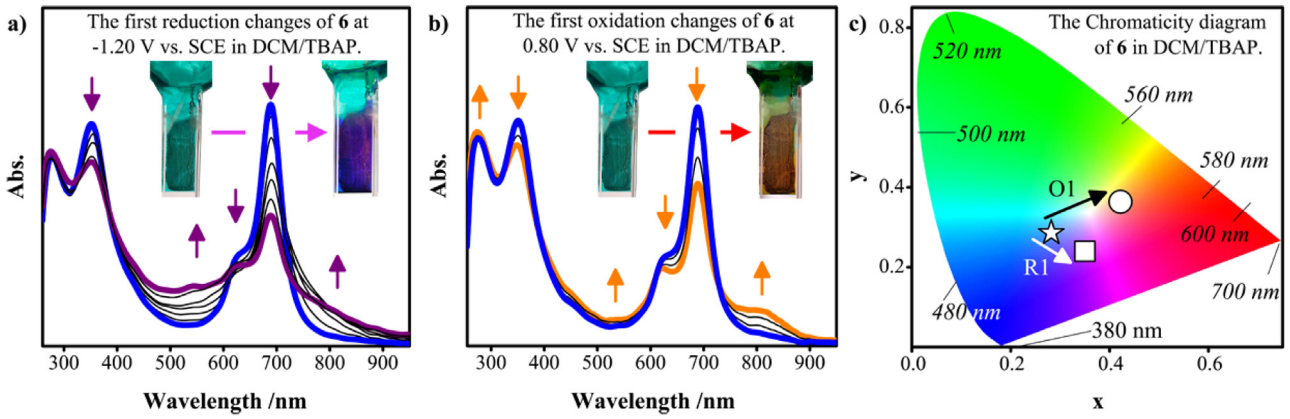

Fig. 9. *In situ* UV-vis spectral changes of ZnPc (6) during the controlled-potential electrolysis in DCM/TBAP electrolyte system at (a) E_{app}= −1.20 V (b) E_{app}= 0.80 V (c) the chromaticity diagram with the color changes of ZnPc (6).

species. After the first oxidation process, the light orange color was obtained, and it was presented on the chromaticity diagram with a circle emblem ($x = 0.422$, $y = 0.364$) in Fig. 9b and c.

Electrochemical and spectroelectrochemical investigations suggested that iron and manganese metal centers in Fe(OAc)Pc (3) and Mn(OAc)Pc (4) respectively, are in the oxidation states of +3, whereas the cobalt metal center in CoPc (2) has an oxidation state of +2. Furthermore, oxidation states of the nickel and zinc metals in NiPc (5) and ZnPc (6) complexes, are +2 in Pcs. It was concluded that because of the beginning +3 oxidation states of metals, Fe(OAc)Pc (3) and Mn(OAc)Pc (4) complexes have exceedingly more affluent redox properties when compared to CoPc (2). Moreover, for the same reason, complexes Fe(OAc)Pc (3) and Mn(OAc)Pc (4) were observed to possess palpably imitative spectroelectrochemical and electrocolorimetric properties. Although cobalt has a + 2 valence state in the Pc complex, spectroelectrochemical and electrocolorimetric results of this compound reveal similarities when compared with Fe(OAc)Pc (3) and Mn(OAc)Pc (4). It demonstrates entirely analogous first reduction and oxidation demeanors as they occur on the redox-active metals that are centered in the Pc ring. When the charge transfer transition energies of CoPc (2), Fe(OAc)Pc (3), and Mn(OAc)Pc (4) complexes are compared respectively 0.92 V, 0.50 V, and 0.68 V, the charge transfer transition energy for the complex Fe(OAc)Pc (3) is pretty lower than the others in DMSO/TBAP solution medium. Furthermore, these findings provide additional information about the comparison between redox inactive metal-centered complexes; for instance, the complex NiPc (5) has better redox properties than the complex ZnPc (6). Metals of both NiPc (5) and ZnPc (6) have no reduction and no oxidation processes; thus, all redox processes belong to Pc rings. HOMO-LUMO gaps of NiPc (5) and ZnPc (6) are pretty close, respectively 1.54 V and 1.55 V in DMSO/TBAP solution medium. With a more positive first reduction process, the NiPc (5) complex has a fairly better redox attitude than the complex ZnPc (6) in DMSO/TBAP solution medium, whereas, with a more negative first oxidation process, the complex ZnPc (6) possesses a better redox feature than NiPc (5). The electrochemical redox properties obtained in the DCM/TBAP solution medium of ZnPc (6) are better than the redox properties of the same complex in the DMSO/TBAP electrolyte system. By comparison of the HOMO-LUMO gap of ZnPc (6) between DCM/TBAP and DMSO/TBAP solution mediums, in DCM/TBAP solution medium; a relatively more positive first reduction and a more negative first oxidation processes were obtained and additionally, the HOMO-LUMO gap is somewhat lower with 1.23 V. Nitrile reductions were observed for all mononuclear Pc complexes in the DMSO/TBAP electrolyte system, except ZnPc (6). In addition, the nitrile reduction for the complex ZnPc (6) was detected in DCM/TBAP electrolyte system. When the square wave voltammograms are analyzed, it can be seen that nitrile reductions have considerably higher current values than other reduction processes due to the reduction of nitrile groups located at four peripheral corner tails of the Pc molecule, as expected. Redox inactive metal centered Pc complexes have closely similar spectroelectrochemical and electrocolorimetric results parallel to the literature in the same electrolyte system.

4. Conclusion

The synthesis and characterization of the metallo (Co, Fe, Mn, Ni, Zn) ball-type phthalocyanine precursors were succeeded by using novel 4,4′-(((4-(tert-butyl)−1,2-phenylene)bis(methylene)) bis(oxy))diphthalonitrile as a starting compound. The novel starting material compound 1 and metallophthalocyanines were specified by classical spectroscopic techniques such as elemental analyses, FT-IR, UV-*vis*, and MALDI-TOF mass. All the Pcs (2–6) were fairly soluble in common organic solvents, such as DCM, chloroform, toluene, DMF, DMSO, and THF. The ball-type phthalocyanine precursors planned to be used as starting materials in the synthesis of -CH_2O- bridged ball-type Pc compounds are the first examples in this field as extended oxo-bridged mononuclear Pcs. In this study, although the longer oxo (-CH_2O-) bridge did not have much effect on the physical, chemical, and spectral properties of Pcs, it is expected that the above-mentioned features will change, as the distance between the cofacial Pc units will increase in -CH_2O- bridged ball-type Pcs which are planned to be synthesized from later.

It can be deduced from voltammetric, *in situ* electrocolorimetric, and *in situ* spectroelectrochemical analysis of CoPc (2), Fe(OAc)Pc (3), Mn(OAc)Pc (4), NiPc (5), and ZnPc (6) in nonaqueous media that these mononuclear Pc compounds usually displayed reversible, Pc ring- and/or central redox active metal-based serial one-electron reduction and oxidation processes. It was observed that due to the redox-active nature of their metal centers, CoPc (2), Fe(OAc)Pc (3), and Mn(OAc)Pc (4) showed richer redox redox behavior with additional redox processes than that of NiPc (5), and ZnPc (6). Therefore, the complexes with redox active metal centers were more easily reduced and oxidized with respect to the others. The complexes also had nitrile reductions that enhanced the redox properties. The high electrochemical performance of the complexes recommended that the complexes have the potential of displaying high electrocatalytic activity, and thus, they can be utilized as functional electrocatalysts for various electron transfer processes, for instance for oxygen reduction. Electrocatalytic performance of these complexes will be evaluated in our future reports after the

completion of our ongoing studies. Furthermore, *in situ* spectroelectrochemical evaluations provided support for a complete decision on the nature of the redox processes of the complexes, *i.e.*, the applicability of their electron transfer processes for color change. Their intense absorption peaks and net color changes through the redox processes showed that they also have the potential for usage as electrochromic materials.

Declaration of Competing Interest

The authors declare that they have no known competing financial interests or personal relationships that could have appeared to influence the work reported in this paper.

CRediT authorship contribution statement

Safinaz Şahin: Conceptualization. **Özgün Akdağ:** Conceptualization. **Efe Baturhan Orman:** Writing – original draft. **Zafer Odabaş:** Writing – original draft. **Ali Rıza Özkaya:** Writing – review & editing.

Data availability

Data will be made available on request.

Acknowledgments

We are grateful to the Scientific and Technological Research Council of Turkey (TUBITAK) for their financial support for the 1001 research project numbered 118Z250 and the Research Foundation of Marmara University, Commission of Scientific Research (BAPKO) for their support of this research as part of the projects: FEN-C-DRP-100719–0249 (Project ID: 2072) and FEN-C-DRP-120917–0545 (Project ID: 1773). A.R. Özkaya also thanks the Turkish Academy of Sciences, TUBA for partial financial support.

Supplementary materials

Supplementary material associated with this article can be found, in the online version, at doi:10.1016/j.molstruc.2022.134769.

References

[1] N.B. McKeown, Phthalocyanine Materials: Synthesis, Structure and Function, Cambridge University Press, 1998.
[2] G. de la Torre, C.G. Claessens, T. Torres, Phthalocyanines: old dyes, new materials. Putting color in nanotechnology, Chem. Commun. (20) (2007) 2000–2015.
[3] M.D. Zhang, D.H. Si, J.D. Yi, Q. Yin, Y.B. Huang, R. Cao, Conductive phthalocyanine-based metal-organic framework as a highly efficient electrocatalyst for carbon dioxide reduction reaction, Sci. China Chem. 64 (8) (2021) 1332–1339.
[4] O.A. Melville, T.M. Grant, B. Mirka, N.T. Boileau, J. Park, B.H. Lessard, Ambipolarity and air stability of silicon phthalocyanine organic thin-film transistors, Adv. Electron. Mater. 5 (8) (2019) 1900087.
[5] D.O. Oluwole, A.V. Yagodin, N.C. Mkhize, K.E. Sekhosana, A.G. Martynov, Y.G. Gorbunova, A.Y. Tsivadze, T. Nyokong, First example of nonlinear optical materials based on nanoconjugates of sandwich phthalocyanines with quantum dots, Chem. A Eur. J. 23(12) (2017) 2820–2830.
[6] A. Wang, J. Ye, M.G. Humphrey, C. Zhang, Graphene and carbon-nanotube nanohybrids covalently functionalized by porphyrins and phthalocyanines for optoelectronic properties, Adv. Mater. 30 (17) (2018) 1705704.
[7] C. Bilen Şentürk, A.N. Şahin, A. Çetin, A. Altındal, Z. Odabaş, Nitrate ion sensing properties of peripheral 3, 4, 5-trimethoxyphenoxy and chlorine substituted metallo and metal-free phthalocyanines, J. Inorg. Organomet. Polym. Mater. 32 (4) (2022) 1436–1447.
[8] R.O. Ogbodu, T. Nyokong, The effect of ascorbic acid on the photophysical properties and photodynamic therapy activities of zinc phthalocyanine-single walled carbon nanotube conjugate on MCF-7 cancer cells, Spectrochim. Acta Part A Molecular Biomol. Spectrosc. 151 (2015) 174–183.
[9] J. Yang, J. Tao, T. Isomura, H. Yanagi, I. Moriguchi, N. Nakashima, A comparative study of iron phthalocyanine electrocatalysts supported on different nanocarbons for oxygen reduction reaction, Carbon 145 (2019) 565–571.
[10] D. Akyüz, A. Koca, Phthalocyanine-aniline dyad constructed with click electrochemistry: a novel hybrid electrochromic material, J. Solid State Electrochem. 24 (2) (2020) 431–440.
[11] S.I. Büyükekşi, E.B. Orman, N. Acar, A. Altındal, A.R. Özkaya, A. Şengül, Electrochemical, photovoltaic and DFT studies on hybrid materials based on supramolecular self-assembly of a ditopic twisted perylene diimide with square-planar platinum (II)-and/or palladium (II)-2, 2′: 6′, 2 ″-terpyridyl complex ions, Dyes Pigment. 161 (2019) 66–78.
[12] A. Kumar, V.K. Vashistha, D.K. Das, Recent development on metal phthalocyanines based materials for energy conversion and storage applications, Coord. Chem. Rev. 431 (2021) 213678.
[13] A. Şenocak, E. Demirbaş, M. Durmuş, Phthalocyanine-nanocarbon materials and their composites: preparation, properties, and applications, in: Nanocarbon and its Composites, Elsevier, 2019, pp. 677–709.
[14] A.Y. Tolbin, A.V. Ivanov, L.G. Tomilova, N.S. Zefirov, Preparation of 1, 2-bis (3, 4-dicyanophenoxymethyl) benzene and the binuclear zinc phthalocyanine derived from it, Mendeleev Commun. 12 (3) (2002) 96–97.
[15] A.Y. Tolbin, A.V. Ivanov, L.G. Tomilova, N.S. Zefirov, Synthesis of 1, 2-bis (3, 4-dicyanophenoxymethyl) benzene and binuclear zinc phthalocyanines of clamshell and ball types, J. Porphyr. Phthalocyanines 7 (03) (2003) 162–166.
[16] Ö. Bekaroğlu, Ball-type phthalocyanines: synthesis and properties, Funct. Phthalocyanine Mol. Mater. (2010) 105–136.
[17] Z. Odabaş, A. Altındal, A.R. Özkaya, M. Bulut, B. Salih, Ö. Bekaroğlu, Synthesis, characterization, and electrochemical and electrical properties of novel mononuclear and binuclear ball-type Zn (II) and Co (II) phthalocyanines substituted with 1a, 8b-dihydronaphtho [b] naphthofuro-[3, 2-d] furan-7, 10-diyl, Polyhedron 26 (14) (2007) 3505–3512.
[18] Z. Odabaş, A. Altındal, B. Salih, M. Bulut, Ö. Bekaroğlu, Synthesis, characterization and electrical properties of novel mono-and cofacial bisphthalocyanines bridged with four [1a, 8b-dihydronaphtho [b] naphthofuro [3, 2-d] furan-7, 10-diyl] units, Tetrahedron Lett. 48 (36) (2007) 6326–6329.
[19] Z. Odabaş, A. Altındal, A.R. Özkaya, B. Salih, Ö. Bekaroğlu, Novel ball-type homo-and hetero-dinuclear phthalocyanines with four 1, 1′-methylenedinaphthalen-2-ol bridges: synthesis and characterization, electrical and gas sensing properties and electrocatalytic performance towards oxygen reduction, Sensors Actuators B Chem. 145 (1) (2010) 355–366.
[20] Z. Odabaş, F. Dumludağ, A.R. Özkaya, S. Yamauchi, N. Kobayashi, Ö. Bekaroğlu, Novel homo-and heterobinuclear ball-type phthalocyanines: synthesis and electrochemical, electrical, EPR and MCD spectral properties, Dalton Trans. 39 (35) (2010) 8143–8152.
[21] M.S. Ağırtaş, A. Altındal, B. Salih, S. Saydam, Ö. Bekaroğlu, Synthesis, characterization, and electrochemical and electrical properties of novel mono and ball-type metallophthalocyanines with four 9, 9-bis (4-hydroxyphenyl) fluorene, Dalton Trans. 40 (13) (2011) 3315–3324.
[22] E. Kakı, A. Altındal, B. Salih, Ö. Bekaroğlu, Synthesis, characterization and gas sensing properties of novel homo and hetero dinuclear ball-type phthalocyanines, Dalton Trans. 44 (17) (2015) 8293–8299.
[23] A.S. Başak, A.R. Özkaya, A. Altındal, B. Salih, A. Şengül, Ö. Bekaroğlu, Synthesis, characterization, oxygen electrocatalysis and OFET properties of novel mono-and ball-type metallophthalocyanines, Dalton Trans. 43 (15) (2014) 5858–5870.
[24] M. Canlıca, A. Altındal, A.R. Özkaya, B. Salih, Ö. Bekaroğlu, Synthesis, characterization, and electrochemical, and electrical measurements of novel 4,4′-isopropylidendioxydiphenyl bridged bis and cofacial bis-metallophthalocyanines (Zn,Co), Polyhedron 27 (7) (2008) 1883–1890.
[25] Z. Odabaş, İ. Koç, A. Altındal, A.R. Özkaya, B. Salih, Ö. Bekaroğlu, Synthesis and electrochemical, *in situ* spectroelectrochemical, electrical and gas sensing properties of ball-type homo-and hetero-dinuclear phthalocyanines with four [1a, 8b-dihydronaphtho [b] naphthofuro [3, 2-d] furan-7, 10-diyl] bridges, Synth. Met. 160 (9–10) (2010) 967–977.
[26] D. Gounden, G. Ngubeni, M. Louzada, S. Khene, J. Britton, N. Nombona, Synthesis, spectroscopic and DFT characterization of 4β-(4-tert-Butylphenoxy)phthalocyanine positional isomers for non-linear optical absorption, S. Afr. J. Chem. 70 (2017).
[27] N. Silva, C. Castro-Castillo, M.P. Oyarzún, S. Ramírez, C. Gutierrez-Ceron, J.F. Marco, J.F. Silva, J.H. Zagal, Modulation of the electrocatalytic activity of Fe phthalocyanine to carbon nanotubes: electrochemistry of l-cysteine and l–cystine, Electrochim. Acta 308 (2019) 295–306.
[28] E.B. Orman, A. Koca, A.R. Özkaya, İ. Gürol, M. Durmuş, V. Ahsen, Electrochemical, Spectroelectrochemical, and Electrochromic Properties of Lanthanide Bis-Phthalocyanines, J. Electrochem. Soc. 161 (6) (2014) H422–H429.
[29] Y. Bian, L. Su, Z. Yu, Z. Lv, H. Chen, Y. Zhou, C. Meng, H. Du, M. Cai, H. Cao, M.-.C. Lin, Graphite/copper phthalocyanine composite cathode for overcharge protection and gas evolution suppression in aluminum-ion batteries at room temperature, Electrochim. Acta 332 (2020) 135188.
[30] H.Y. Yenilmez, Ö. Akdağ, A.M. Sevim, A. Koca, Z.A. Bayır, Electrochemical, spectroelectrochemical characterization and electropolymerization of 2-(4-methyl-1,3-thiazol-5-yl)ethoxy-substituted manganese and indium phthalocyanines, Polyhedron 99 (2015) 244–251.
[31] S.R. Nxele, D.O. Oluwole, T. Nyokong, Electrocatalytic activity of a push pull Co(II) phthalocyanine in the presence of graphitic carbon nitride quantum dots, Electrochim. Acta 326 (2019) 134978.
[32] E.B. Orman, Z. Odabaş, A.R. Özkaya, High electrochemical versatility and applicability with metal phthalocyanines carrying peripheral 2,3-dihydro-1H-inden-5-yloxy Substituents: rich redox behavior, oxygen electrocatalysis and electrochromism, J. Electrochem. Soc. 165 (9) (2018) h530–h548.
[33] E.B. Orman, S. Altun, Z. Odabaş, A. Altındal, A.R. Özkaya, Electrochemical, electrocatalytic dioxygen reducing and dielectric relaxation properties of Non-pe-

ripheral Tetra-2,3-dihydro-1H-inden-5-yloxy substituted phthalocyanines, J. Electrochem. Soc. 162 (12) (2015) h825–h840.
[34] F. Yoshii, T. Nakamura, S. Hirono, Y. Shimizu, T. Hoshi, M. Ando, H. Hagiwara, Conformational analysis and selection of odor-active conformers: synthesis of molecules designed for the lily-of-the-valley(Muguet)-type odor, Helv. Chim. Acta 84 (7) (2001) 2051–2063.
[35] S.G. Feridun, E.B. Orman, Ü. Salan, A.R. Özkaya, M. Bulut, Synthesis, characterization, and electrochemical and *in-situ* spectroelectrochemical properties of novel peripherally and non-peripherally 7-oxy-3-(3,4-dimethoxyphenyl) coumarin substituted phthalocyanines, Dyes Pigment. 160 (2019) 315–327.
[36] J. Janczak, R. Kubiak, M. Śledź, H. Borrmann, Y. Grin, Synthesis, structural investigations and magnetic properties of dipyridinated manganese phthalocyanine, MnPc (py) 2, Polyhedron 22 (19) (2003) 2689–2697.
[37] L. Meng, K. Wang, Y. Han, Y. Yao, P. Gao, C. Huang, W. Zhang, F. Xu, Synthesis, structure, and optical properties of manganese phthalocyanine thin films and nanostructures, Prog. Nat. Sci. Mater. Int. 27 (3) (2017) 329–332.
[38] A.T. Bilgicli, M. Kandaz, A.R. Ozkaya, B. Salih, Tetrakis-phthalocyanines bearing electron-withdrawing fluoro functionality: synthesis, spectroscopy, and electrochemistry, Heteroat. Chem. 20 (5) (2009) 262–271.
[39] E. Baturhan Orman, M.B. Sağlam, A.R. Özkaya, Novel peripherally substituted metal-free, zinc (II), and cobalt (II) phthalocyanines with 1,1'-thiobis(2-napthol) and additional tetraphthalonitrile groups: synthesis, aggregation behavior, electrochemical redox and electrocatalytic oxygen reducing properties, Synth. Met. 263 (2020) 116351.
[40] İ. Günay, E.B. Orman, A. Altındal, B. Salih, M. Özer, A.R. Özkaya, Novel tetrakis 4-(hydroxymethyl)-2,6-dimethoxyphenoxyl substituted metallophthalocyanines: synthesis, electrochemical redox, electrocatalytic oxygen reducing, and volatile organic compounds sensing and adsorption properties, Dyes Pigment. 154 (2018) 172–187.
[41] Z. Odabaş, E.B. Orman, M. Durmuş, F. Dumludağ, A.R. Özkaya, M. Bulut, Novel alpha-7-oxy-4-(4-methoxyphenyl)-8-methylcoumarin substituted metal-free, Co(II) and Zn(II) phthalocyanines: photochemistry, photophysics, conductance and electrochemistry, Dyes Pigment. 95 (3) (2012) 540–552.
[42] Ü.E. Özen, T. Keleş, Z. Bıyıklıoğlu, A. Koca, A.R. Özkaya, Electropolymerization and electrochemical pesticide sensor application of metallophthalocyanines bearing polymerizable morpholin groups, J. Electrochem. Soc. 163 (14) (2016) b673–b682.
[43] S. Altun, Z. Odabaş, A. Altındal, A.R. Özkaya, Coumarin-substituted manganese phthalocyanines: synthesis, characterization, photovoltaic behaviour, spectral and electrochemical properties, Dalton Trans. 43 (21) (2014) 7987–7997.
[44] H. Yalazan, Y.E. Maden, A. Koca, H. Kantekin, Multi-step syntheses, electrochemistry and spectroelectrochemistry of peripheral CoII, CuII and MnIIICl phthalocyanines bearing pyrazoline, J. Mol. Struct. 1269 (2022) 133788.
[45] B. Köksoy, O. Soyer, E.B. Orman, A.R. Özkaya, M. Bulut, Synthesis, electrochemistry and *in situ* spectroelectrochemistry of novel tetra dimethyl 5-oxyisophthalate substituted Co(II), Mn(III), and μ-oxo-dimer Fe(III) phthalocyanines, in: Dyes Pigment., 118, 2015, pp. 166–175.
[46] H. Yalazan, H. Kantekin, Ö. Budak, A. Koca, Non-peripheral tetra methoxylated pyrazoline bearing CoII, CuII and MnIIICl phthalocyanines: syntheses, electrochemistry and spectroelectrochemistry, J. Organomet. Chem. 973-974 (2022) 122405.
[47] Ü. Demirbaş, D. Akyüz, H.T. Akçay, A. Koca, H. Kantekin, Non-peripherally tetra substituted phthalocyanines bearing benzodioxane moieties: synthesis, characterization and investigation of electrochemical and spectroelectrochemical properties, J. Mol. Struct. 1189 (2019) 234–239.
[48] İ. Değirmencioğlu, M. Er, R. Bayrak, A.R. Özkaya, Redox-switchable new phthalocyanines containing hydrazono-thiazole-carboxylate fragments: synthesis, electrochemical, spectroelectrochemical and electrocolorimetric investigation, J. Fluoresc. 27 (3) (2017) 869–881.
[49] A. Arıbal, E.B. Orman, Ü. Salan, A.R. Özkaya, M. Bulut, Novel peripherally and non-peripherally 6-oxyflavone substituted metal-free, zinc(II) and cobalt(II) phthalocyanines: electrochemical and *in situ* spectroelectrochemical properties, J. Porphyr. Phthalocyanines 22 (01n03) (2018) 279–290.
[50] N. Farajzadeh, D. Akyüz, A. Koca, M.B. Koçak, Synthesis, electrochemistry and *in situ* spectroelectrochemistry of novel tetra- and octa-substituted metallophthalocyanines bearing peripherally 4-(trifluoromethoxy)phenoxy groups, Polyhedron 177 (2020) 114264.
[51] A. Gök, E.B. Orman, Ü. Salan, A.R. Özkaya, M. Bulut, Synthesis, characterization and electrochemical properties of tetra 7-oxy-3-biphenylcoumarin substituted metal-free, zinc(II), cobalt(II) and indium(III) phthalocyanines, Dyes Pigment. 133 (2016) 311–323.